FINAL REPORT

NASA GRANT NSG 5414

Supplement 1

THE RELATIONSHIP OF SENSOR PARAMETERS TO APPLICATIONS DATA ANALYSIS

David A. Landgrebe

Principal Investigator

and

Erick R. Malaret

Purdue Research Foundation

West Lafayette, Indiana 47907

May, 1981 - August, 1982

83N21213

FINAL REPORT

NASA GRANT NSG 5414

Supplement 1

THE RELATIONSHIP OF SENSOR PARAMETERS TO APPLICATIONS DATA ANALYSIS

David A. Landgrebe

Principal Investigator

and

Erick R. Malaret

Purdue Research Foundation

West Lafayette, Indiana 47907

May, 1981 - August, 1982

FINAL REPORT

NASA GRANT NSG 5414

Supplement 1

Mr. Frederick Gordon, Jr./Code 902
NASA GSFC Technical Officer

THE RELATIONSHIP OF SENSOR PARAMETERS TO APPLICATIONS DATA ANALYSIS

May, 1981 - August, 1982

David A. Landgrebe
Principal Investigator

and

Eric Malaret

Purdue Research Foundation
West Lafayette, Indiana 47907

TABLE OF CONTENTS

LIST OF TABLES

LIST OF FIGURES

ABSTRACT

In this thesis a stochastic model for the data acquisition system in a multispectral scanner system, like the one utilized by the LANDSAT satellites, is presented. A list of noise sources which are known or presumed to have a significant effect in the information extraction process was constructed. Since the shot noise introduced by the photodetectors in the sensor system is signal level dependent, an atmospheric model was adopted which could adequately describe the amount of radiation that gets into the sensors based on the atmospheric transmittance. An analysis was carried out to find the output spectral statistics in terms of the input signal statistics and the system parameters. This was integrated into a set of fortran programs that when supplied with, the class statistics, the noise levels introduced by the sensor system, the atmospheric transmittance, and the atmospheric path radiance, can be used to estimate the classification performance. In order to show the beneficts of this model a series of runs were performed in which the Thematic Mapper multispectral scanner was the system under consideration. Consideration was given to the usage of preprocessing spatial filters as a way to combat the noise introduced into the signal at different stages of the system.

CHAPTER 1
INTRODUCTION

1.1 Background

Remoted Sensing of the environment is largely concerned with the measurements of electromagnetic energy emitted or reflected from the earth surface. The data acquisition system can be considered in four basic parts: the radiation source, the atmospheric path, the target, and the sensor. In the case of Landsat, the sun is the radiation source and the atmosphere modifies the spectral distribution of the solar radiance. A portion of the spectral radiance that arrives at the earth surface in the visible and reflective infrared is reflected back through the atmosphere and then may be measured in several spectral bands by a multispectral sensor. Some of the sun's energy is absorbed and then re-emitted at thermal infrared wavelengths. The output of the sensor in each spectral band for a pixel on the earth surface is used to form a point in a n dimensional space. This data is digitized and transmitted to a ground station for processing.

Different ground covers have different spectral reflectance properties. This provides the basis for their identification. Detecting these spectral differences between ground covers allows classification of each pixel of the observed scene as coming from one of a set of possible classes. Due to the randomness of

nature the points from a particular class can be characterized by a stochastic ensemble. Fu, Landgrebe, and Phillips [F3] have shown empirically that a multivariate gaussian density function is a good characterization for agricultural multispectral data. This has imposed the use of statistical pattern-recognition methods in the data analysis. A commonly used pattern classifier algorithm is the minimum Bayes error scheme [S3].

1.2 Statement of the problem

The signal in a remote sensing system is corrupted, at different stages of the data acquisition process, by different noise sources. It would be important to understand the manner in which the different types of noise occurring in a remote sensing system impact the performance of the data analysis portion of the system. This subject has received relatively little attention to this time, and the amount of information available in the literature is rather limited. Studies to date have tended to concentrate primarily on the effect of independent white Gaussian noise on classification accuracy [W1,M1,M2]. Mobasseri developed a parametric model to analytically evaluate the response of a multispectral scanner in any operational environment. In his work the atmospheric effect was not considered, and the noise introduced by the sensor system was arbitrarily chosen; it was assumed to have the same statistical properties over all the spectral bands. Maxwell had also made a system analysis study of the remote sensing system. He discussed the usage of preprocessing the data before any classification is done. Although there have been extensive studies on models for "correcting" or calibrating data in the face of

atmospheric effects [T1], little is known about the deleterious impact of these effects on the process of information extraction. Other system noise sources have received even less attention; thus the relatively broad field of noise sources, the interrelation of them with remote sensing system parameters, and the information extraction process remains unexplored.

If the full potential of current, and especially of planned sensor systems is to be realized, a better delineation of the relationship between sensor parameters and data analysis results is needed.

1.3 Objectives

It is the objective of this work to develop a stochastic system model that can be used to integrate and investigate the effect that different noise sources, introduced by the atmosphere and the sensor system, can have on system performance. Since both the signal and the noise are considered to be random in character and therefore not obviously identifiable by inspection, a suitable definition of the two is needed. The signal is defined to be that portion of the scene response variability which contributes in any way to the ability to discriminate among classes. For example, texture of a given cover class in a given scene may appear to be random. However, in this case the randomness implies variability which might be indicative of the cover class, and thus might be part of the signal. All scene and system response variability which does not so contribute to identifiability is defined to be the noise. The theory of stochastic process models for such situations provides a rich background of well established tools, and these models have been the traditional types of models

used for highly complex problems.

Since the ultimate goal of most systems designed to recognize patterns is to do so accurately, the probability of error is an important index of performance which it is desirable to minimize, although, there is a lower bound on the probability of error imposed by the random nature of the signals. The classifier used is a Bayes minimum error pixel classifier for multivariate gaussian density functions [S3]. In order to provide a measure of specificity to this otherwise very general study, it was decided to use the Thematic Mapper sensor parameters as an example system. In Appendix A a general description of the Thematic Mapper is presented. The next chapter will discuss the different noise sources to be modeled in the system.

CHAPTER 2
NOISE SOURCES

2.1 Noise List

As was mentioned earlier we wish to model scene and system response variabilities in the data acquisition system which can potentially improve the information extraction process. To begin the study a list of noise sources was constructed. This list is intended to include all the sources of noise which are known or presumed to have a significant deleterious effect on the classification of the data. Since it would be impractical to deal with a very extensive list, it was decided to prioritize the list, which is as follows:

Priority 1

1. Atmospheric effect(constant atmosphere)
2. Detector noise process
    a. Shot noise(signal level dependent)
    b. Johnson noise
3. Quantization effect

Priority 2

1. Training statistics estimation error
2. Optically induced noise
3. Atmospheric effect (non-constant atmosphere)
4. Goniometric variations
5. Non-class conditional earth surface variability

In constructing this list consideration was given both to the speculated magnitude of the noise effect on net system performance, and upon the probability of affecting performance improvements by better parameter selection in the system design phase. It was shown by Mobasseri, McGillem, and Anuta [M2] that the noise prior to detection is quite negligible and thus for all practical purposes can be neglected. This implies that random noise generated by the detector and quantizer stages are the major sources of disturbance on the signal. This work is limited to the Priority 1 list. We proceed next with a description of the noise sources in the Priority 1 list.

2.2 Atmospheric Effect

In this section the atmospheric model that was used in the simulation is presented. The atmosphere is known to be a quite complex portion of the system, with a number of mechanisms operative which will affect radiances passing through it. To attempt to model all of these would be prohibitively complex and indeed is not necessary for the purposes of this early stage of

studying the effect of such noise sources. Instead we will use a simple atmospheric model for the preliminary work.

The atmosphere modifies the spectral solar radiance in a wavelength dependent manner by two basic mechanisms, absorption and scattering. The combination of these two is frequently refered to as attenuation. The fundamentals of atmospheric scattering, and absorption involve complexities in mathematical physics beyond the scope of this **work** . The discussion that follows will deal with the topic in a less fundamental manner.

Absorption is the transformation of radiant energy into heat. In a clear (haze free) atmosphere, absorption is almost negligible in many portions of the optical range. For a hazy or polluted atmosphere absorption plays an important role. Atmospheric absorption due to ozone is very strong for wavelengths below .29um .

Scattering occurs when the radiation is reflected or refracted, from its original directional flow, by particles in the atmosphere. There are three basic kinds of scattering mechanism: Rayleigh, Mie, and non-selective scattering. Each of these is based upon the presence of different scattering elements. Certain spectral bands of the solar irradiance that pass through the atmosphere are not severely attenuated. These bands are called atmospheric windows and are widely used by earth observational satellites.

The atmosphere has three basic effects on the data acquisition system. First, the spectral and spatial distribution of the incoming solar radiance (the source) is modified as it passes through the atmosphere. Second, the reflected and/or emitted spectral radiance from the earth surface (the target) is attenuated. Third, a component of scattered radiation called path radiance is added to the attenuated signal. The path radiance also depends on the

reflectivity of the target and its surroundings. For simplicity we will assume that the fields of interest are big enough such that the reflectivity is fairly uniform around the target, even though this assumption is frequently not the case. Kiang [K1] showed that atmospheric effects on the reflected radiance can be approximated with a linear equation, where the spectral radiance that falls within the instantaneous field of view (IFOV) of the multispectral scanner is as a function of wavelength λ, is

$$\mathbf{L}(\lambda) = \tau_a(\lambda)\mathbf{L}_s(\lambda) + L_p(\lambda). \tag{2.1}$$

$\mathbf{L}_s$ (the signal) is the reflected and/or emitted spectral radiance from the pixel under observation, $\tau_a(\lambda)$ is the spectral atmospheric transmittance, and L_p is the path spectral radiance introduced by scattering. Both $\mathbf{L}_s$ and $\mathbf{L}$ are known to be random variables that are functions of the wavelength. Although it is not written explicitly τ_a, $\mathbf{L}_s$, and L_p are functions of the solar zenith angle (θ) and the metereological range or visibility (V_η). We are assuming that the ground is a Lambertian surface, which implies that the reflected radiance is independent of the viewing angle.

The spectral transmittance from the earth surface into the outer atmosphere is given by

$$\tau_a(\lambda, V_\eta, \theta) = e^{-\tau'_{ext}(\lambda, V_\eta)\sec\theta}, \tag{2.2}$$

where τ'_{ext} is the extinction optical thickness introduced by ozone absorption, Rayleigh, and aerosol scattering. Elterman [E1] has done experimental and

Table 2.1 Atmospheric extinction optical thickness for eight metereological ranges and twenty different wavelengths in the range of .27-2.17 um.

Extinction Optical Thickness τ'_{ext}								
$\lambda(\mu m)$	Metereological Range V_η(km)							
	2	3	4	5	6	8	10	13
0.27	76.276	75.324	74.825	74.513	74.299	74.020	73.847	73.681
0.28	40.658	39.760	39.289	38.995	38.794	38.530	38.368	38.211
0.30	7.657	6.809	6.364	6.086	5.896	5.647	5.493	5.345
0.32	4.080	3.281	2.863	2.601	2.422	2.187	2.042	1.903
0.34	3.414	2.665	2.273	2.027	1.859	1.639	1.503	1.372
0.36	3.086	2.383	2.014	1.783	1.625	1.418	1.291	1.167
0.38	2.881	2.202	1.847	1.624	1.472	1.272	1.149	1.030
0.40	2.593	1.969	1.642	1.437	1.297	1.114	1.000	.891
0.45	2.203	1.650	1.360	1.178	1.054	.891	.791	.694
0.50	1.968	1.462	1.197	1.031	.917	.768	.676	.587
0.55	1.805	1.337	1.092	.939	.834	.696	.611	.529
0.60	1.624	1.204	.984	.846	.751	.627	.551	.477
0.65	1.452	1.069	.868	.742	.655	.542	.473	.405
0.70	1.341	.982	.793	.675	.594	.488	.423	.359
0.80	1.178	.859	.692	.588	.516	.422	.364	.307
0.90	1.067	.777	.624	.529	.463	.378	.325	.273
1.06	.961	.699	.561	.475	.416	.338	.290	.244
1.26	.876	.637	.511	.433	.379	.308	.264	.222
1.67	.753	.548	.441	.373	.326	.266	.228	.192
2.17	.672	.489	.392	.332	.290	.236	.202	.169

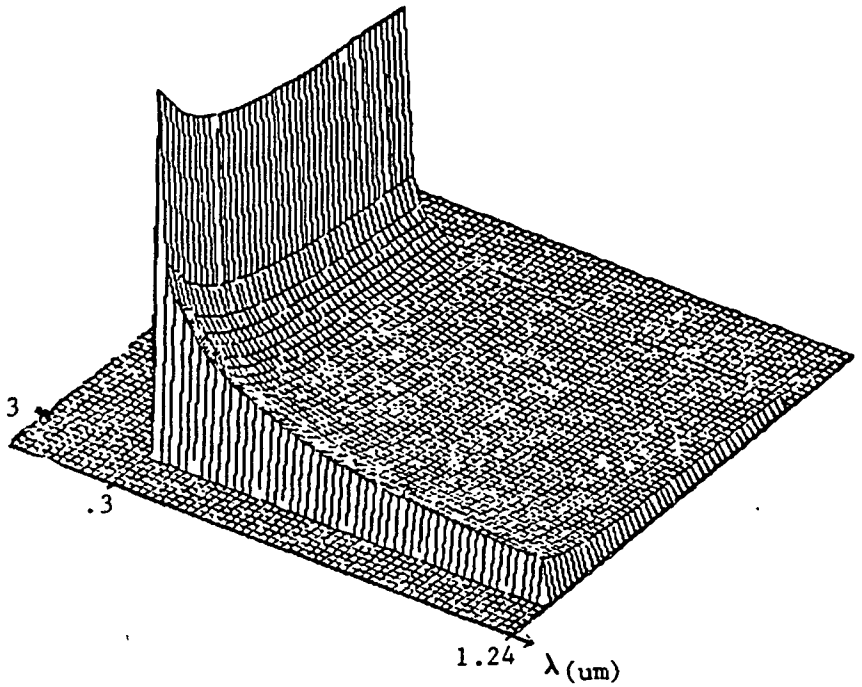

Figure 2.1 Atmospheric optical thickness as a function of wavelenght and metereological range.

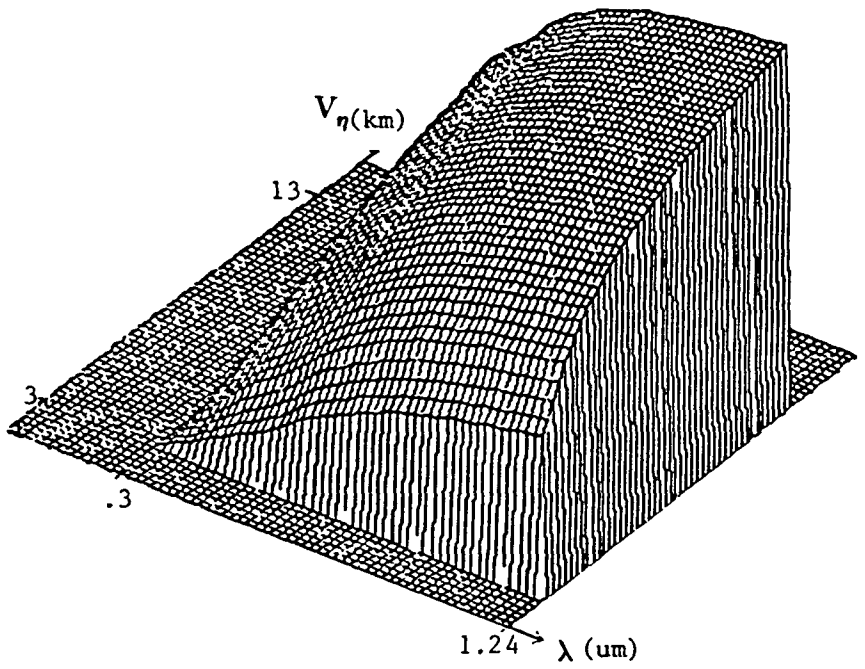

Figure 2.2 Atmospheric transmittance as a function of metereological range and wavelength.

theoretical tabulations of spectral optical parameters for a hazy atmosphere with different metereological ranges. A selected part of Elterman's tabulations for τ'_{ext} are presented in Table 2.1. Using this table a satisfactory linear interpolation can be made between the wavelengths of .27um and about 1um, because τ'_{ext} is a slowly varying function of the wavelength. Fig. 2.1 is the result of interpolating over the wavelength range of .3-1.24 microns and over the metereological range of 2 to 13 kilometers. Fig. 2.2 is the atmospheric transmittance obtained from (2.2) for a solar zenith angle of 37.5 degrees and optical thickness given by Fig. 2.1. Observe that atmospheric attenuation is stronger in the blue wavelength region compared to the red wavelength region. This accounts for having reddish sunsets.

There are different models to estimate the atmospheric path radiance. I will adopt in this work Duntley's method [D2], because of its simplicity compared to other existing methods [S2]. Duntley argued that each segment of the atmosphere has an equilibrium radiance L_{eq} with a path radiance given by

$$L_p(\lambda) = L_{eq}(\lambda)[1 - \tau_a(\lambda, V_\eta, \theta)]. \tag{2.3}$$

In this method the equilibrium radiance can be determined from ground based radiance and transmittance measurements.

Landsat photodetectors respond to the radiation that lies within certain narrow spectral bands. Since we are only using a finite number of spectral bands a matrix formulation of (2.1) is required.

$$\begin{bmatrix} L_1 \\ L_2 \\ \\ L_n \end{bmatrix} = \begin{bmatrix} \tau_{a_1} & & & \\ & \tau_{a_2} & 0 & \\ & 0 & & \\ & & & \tau_{a_n} \end{bmatrix} \begin{bmatrix} L_{s_1} \\ L_{s_2} \\ \\ L_{s_n} \end{bmatrix} + \begin{bmatrix} L_{p_1} \\ L_{p_2} \\ \\ L_{p_n} \end{bmatrix} \tag{2.4}$$

$$\underline{\mathbf{L}} = \underline{\tau_a \mathbf{L}_s} + \underline{\mathbf{L}_p}.$$

$\mathbf{L}_i$ is the radiance that enters the pupil of the sensor in the wavelength range covered by the i^{th} channel of the sensor. For notational simplicity τ_a, L_p, and $\mathbf{L}_s$ will be refered to from now on as the transmittance matrix, the equivalent radiance vector and the signal vector, respectively.

A linear transform of the form of (2.4) does not of itself affect the classification results obtained from a minimum error Bayes classifier for multivariate gaussian distributions. This can be shown as follows. Denote the density function of the reflected radiance for class w_j before it passes through the atmosphere as

$$p(\mathbf{L}_s | w_j) = N(M_j, \Sigma_j) \tag{2.5}$$

that is, a multivariate gaussian density function with covariance matrix Σ_j and mean vector M_j . The density function of the received radiance is given by

$$p(\mathbf{L} | w_j) = N(\tau_a M_j + L_p , \tau_a \Sigma_j \tau_a^t). \tag{2.6}$$

Using (2.4) it is a matter of substitution to show

$$p(\mathbf{L}|\, w_j) = \frac{1}{|\tau_a|}\, p(\mathbf{L}_s|\, w_j). \tag{2.7}$$

Since the transformed density function differs from its original density by a multiplicative constant, the classification statistics in a multiclass problem are unaffected. It can also be shown that the correlation coefficients between channels is also preserved by (2.4),

$$\rho'_{ij} = \rho_{ij}. \tag{2.8}$$

Thus the probability of misclassification between two different classes remain the same after going through the atmosphere. This is true as long as an ideal sensor and a constant atmosphere are considered.

A plausible atmospheric model has been introduced in this section. The inputs to the model are: the atmospheric transmittance matrix and the path radiance vector. It is important to recognize that this model is deterministic in nature and does not account for spatial, spectral, and temporal atmospheric variations. In Appendix B a non constant atmospheric model is discussed.

2.3 Shot Noise

The purpose of this section is to find the first order statistics of the shot noise introduced by the photodetectors in the sensor system. Shot noise processes were first studied in connection with phototubes, but they have also been observed in solid states devices like photodiodes [D1].

A photodetector converts light intensity into a current or voltage waveform. When light with the proper wavelength is received at the surface of the photosensitive material, electrons are released from its inner surface and pulled by an electric field to a collecting anode. The flow of a single electron from the cathode to the anode produces a current pulse, h(t), at the photodetector output. This pulse is of finite duration and area equal to one electron charge [D1]. If an electromagnetic field is received at the surface of the photodetector at time t=0, the output response current of the photodetector is the sum of a random number of randomly located response functions h(t),

$$x(t) = \sum_{n=0}^{k(0,t)} h(t-t_n) \quad t \geq 0, \tag{2.9}$$

where t_n is the time of release of the n^{th} electron and k(0,t), the counting process, is the number of electrons released during the time interval (0,t). Both k(0,t) and t_n are random variables. A process like the one describe by (2.9) is called a shot noise process. In order to find the statistics of this process, specification of the statistics of the emission times $\{t_n\}$ and the counting process k(0,t) are required .

The electron count is the number of electrons that flow during a particular interval when detecting a radiation field with a photoresponsive surface. Given a constant irradiance field the probability of releasing k electrons from the photodetecting surface during the interval of time T is [R1],

$$P(k) = \frac{m^k}{k!}e^{-m} \qquad k=0,1,2,... \tag{2.10}$$

K has a Poisson distribution with parameter m. The parameter m is called the level of the probability and is directly proportional to the radiance level L that strikes the photodetector surface area A.

$$m = \gamma L. \tag{2.11}$$

γ is a proportionality constant between the field intensity and the count intensity. It is important to mention that γ is a function of the surface area A of the photodetector, the detector quantum efficiency, and the counting interval T. The characteristic function of the discrete random variable k is given by

$$\Phi(w) = E[e^{jwk}] = \sum_{k=0}^{\infty} e^{jwk}P_k(k) \tag{2.12}$$

$$= e^{-m}\sum_{k=0}^{\infty}\frac{m(e^{jw})^k}{k!} = \exp[m(e^{jw}-1)].$$

It is well known that the characteristic function of a random variable can be used to find the moments of the corresponding random variable [P1],

$$E[k^n] = -j^n \left[\frac{d^n}{dw^n} [\Phi_k(w)] \right]_{w=0} . \tag{2.13}$$

From (2.12) and (2.13) it follows that the first two moments and the variance for the counting process k are

$$E[k] = m \tag{2.14}$$

$$E[k^2] = m^2 + m$$

$$\sigma_k^2 = m.$$

Rice [R1] showed that the electron emission times in the photodetector are independent identically distributed random variables with uniform density functions over the interval $(t, t+T)$,

$$p(t_n) = \begin{cases} \frac{1}{T} & t \leq t_n \leq t+T \\ 0 & \text{elsewhere} \end{cases} . \tag{2.15}$$

Knowing the first order statistics of the counting process and the emission times, an expression for the density function of the Poisson shot noise process can be found,

$$p_x(x(t)) = \frac{1}{2\pi} \int_{-\infty}^{\infty} \Phi_x(w,t) e^{-jwx(t)} dw, \tag{2.16}$$

where the characteristic function of the shot noise, $\Phi_x(w,t)$, is given by

$$\Phi_x(w,t) = E[e^{jwx(t)}] = E_k(E_{t_n}[\exp(jw\sum_{n=0}^{k} h(t-t_n))|\, k]). \tag{2.17}$$

Since the t_n's are independent,

$$\Phi_x(w,t) = E_k(\prod_{n=1}^{k} E_{t_n}[(e^{jwh(t-t_n)}]) = E_k[\Phi_y^k(w,t)]$$

where $\Phi_y(w,t)$ is defined as

$$\Phi_y(w,t) = E_{t_n}[e^{jwh(t-t_n)}].$$

Taking the expected value with respect to k and making use of (2.12),

$$\Phi_x(w,t) = \sum_{k=0}^{\infty} \Phi_y^k(w,t)P(k) = \exp([\Phi_y(w,t)-1]m).$$

(2.17) is a general result given that a constant radiance is getting into the sensor. Without loss of generality, let us define the response function, h(t), as being equal to

$$h(t) = \begin{cases} \dfrac{q_e}{\tau_h} & 0 \le t \le \tau_h \\ 0 & \text{elsewhere} \end{cases}$$

where q_e is electron charge and τ_h is the pulse duration time, then

$$\Phi_y(w)-1 = \frac{\tau_h}{T}[\exp(jw\frac{q_e}{\tau_h})-1] \tag{2.18}$$

$$\Phi_x(w) = \exp[n\tau_h(e^{jw\frac{q_e}{\tau_h}}-1)]$$

where, $n = \frac{m}{T}$, is known as the count intensity. For this particular realization of h(t), $\Phi_x(w)$ is no longer a function of t. Again, the expected value of x and its variance can be found using the characteristic function $\Phi_x(w)$,

$$E(x) = -j\frac{d\Phi_x}{dw}\Big|_{w=0} = q_e n = q_e\frac{m}{T} = (\frac{q_e\gamma}{T})L \tag{2.19}$$

$$\sigma_x^2 = \frac{nq_e^2}{\tau_h} = (\frac{q_e^2\gamma}{\tau_h T})L.$$

Observe, E(x) and σ_x^2 are both dependent on the received intensity. When the received intensity is high, the spread of the shot noise (its standard deviation) is small compare to E(x). In order to find an approximation to the shot noise density function let us define the normalized shot noise process as x_n

$$x_n = \frac{x-E(x)}{\sigma_x} \tag{2.20}$$

$$\Phi_{x_n}(w) = \Phi_x(\frac{w}{\sigma_x})e^{-j\frac{E(x)}{\sigma_x}} \tag{2.21}$$

$$= \exp[-jw\sqrt{n\tau_h} + \sum_{q=1}^{\infty}(jw)^q(n\tau_h)^{1-\frac{q}{2}}].$$

This last expression can easily be shown to converge to (2.22) as $n\tau_h \to \infty$

$$\Phi_{x_n}(w) \simeq \exp[-\frac{w^2}{2}]. \tag{2.22}$$

Since the normalize process x_n is related to x by (2.20) it follows that x approximates a gaussian random variable with mean E(x) and variance σ_x^2 provided $n\tau_h >> 1$,

$$p_x(x) \simeq \frac{1}{\sqrt{2\pi\sigma_x^2}}\exp(\frac{-(x-E(x))^2}{2\sigma_x^2}). \tag{2.23}$$

Gagliardi [G1], proved that this approximation is independent of the shape of h(t) as long as

$$n\tau_h >> 1 \tag{2.24}$$

and

$$\int_{-\infty}^{\infty} h^q(t)dt < \infty \quad \text{for all } q > 2.$$

$n\tau_h$ is physically related to the number of electrons emitted during the interval

$(0,\tau_h)$ or in terms of the input radiance,

$$n\tau_h = (\frac{\tau_h \gamma}{T})L.$$

When the condition $n\tau_h >> 1$ is not satisfied, the discrete nature of the Poisson shot noise process will be evident at the photodetector output and a closed form representation for the density function (2.16) becomes very complicated.

As was discussed in Chapter 1 the pixel radiance L from a given class and spectral band is a random variable. For a given pixel, L can be assumed constant because during the period of time that the measurement is done; there is no significant variation in the radiance being received by the photodetector. This suggest that in Landsat's case what we have is a conditional Poisson shot noise process for every pixel observed on the earth surface. When this is the case, the characteristic function in (2.21) becomes a conditional characteristic function, conditioned over the random variable L. If the values assumed by L still satisfying the conditions of (2.24) then the conditional density function of the photodetector output will be (2.23) conditioned over L. For every observed pixel the output of the photodetector could be modeled as the pixel constant intensity level, the signal, plus a random variation from this intensity, the noise. This random variation or noise is normal with a zero mean value and a variance that is proportional to the (signal) intensity level. A model like this suggests looking at the shot noise process as a signal plus noise problem. There is one difficulty with this interpretation that must be kept in mind; it is the fact that both the signal and the noise are not strictly independent.

It can be shown that the noise at the photodetector output is uncorrelated to the signal level; remember that two process can be uncorrelated but still not

independent. This is the case here. Since the noise in one channel is uncorrelated to the signal level in that channel, and different detectors are used for different wavelengths bands, the noise between the different photodetectors is uncorrelated.

In this section the basis for the noise introduced by the photodetector was presented with an approximation for the density function of the photodetector output when the received signal level is high.

2.4 Quantization Noise

For Landsat satellites, the data undergoes an A/D conversion before it is transmitted to an earth ground station. A/D conversion involves the quantization of the analog signal to $q=2^n$ levels , where n is the number of bits available. Basically, quantization is a mapping of the continuous data sample space into a finite number of selected values. Once the signal is quantized it can not be recovered exactly as it was before quantization. Since the quantization process introduces some fluctuation about the true signal value, this fluctuations can be regarded as an additive noise. The quantizer noise is defined as

$$\epsilon = x - x_q, \tag{2.25}$$

x is the signal, and x_q is the quantized signal. The mean square error introduced by the quantizer is given by [G2]

$$\overline{\epsilon^2} = \sum_{i=1}^{q} \int_{I_i} (x-x_i)^2 p(x \mid i) dx P_i = \sum_{i=1}^{q} \int_{I_i} (x-x_i)^2 p(x) dx, \tag{2.26}$$

where I_i is the i^{th} interval range, $p(x|i)$ is the probability density of the sample value when in I_i , and x_i is the quantization value of the i^{th} interval.

When a uniform quantizer is used and the conditional density function of the input is uniform over all intervals, the error ϵ has a uniform distribution over one quantization interval Δ ,

$$p(\epsilon) = \begin{cases} \frac{1}{\Delta} & -\frac{\Delta}{2} \leq \epsilon \leq \frac{\Delta}{2} \\ 0 & \text{elsewhere} \end{cases} \tag{2.27}$$

and its mean square error is given by

$$\overline{\epsilon^2} = \frac{\Delta^2}{12}. \tag{2.28}$$

If the signal to be quantized has a normal distribution with zero mean and variance σ^2 and a uniform quantizer with 2^q levels is used the mean square error is given by

$$\overline{\epsilon^2} = \frac{2}{\sigma\sqrt{2\pi}} \left[\sum_{i=0}^{\frac{q}{2}-2} \int_{i\Delta}^{(i+1)\Delta} (x-i\Delta-\frac{\Delta}{2})^2 e^{\frac{-x^2}{2\sigma^2}} dx + \int_{(\frac{q}{2}-1)\Delta}^{\infty} (x-\frac{q}{2}\Delta+\frac{\Delta}{2})^2 e^{-\frac{x^2}{2\sigma^2}} dx \right]. \tag{2.29}$$

Since the signal in Landsat satellites is usually modeled by a gaussian distribution, (2.29) is a more exact expression to describe the mean square error

introduced by the quantizer. From (2.29) it can be observed $\overline{\epsilon^2}$ is a function of the signal variance. A computation of the mean square error (mse) and signal to noise ratio (SNR) was carried out for different standard deviations with the number of quantization levels fixed to 256, which corresponds to the Thematic Mapper quantizer system. This was done for gaussian and uniform density functions. The results obtained are shown in Fig. 2.3 and 2.4, which clearly show that for standard deviations in the range of .5 to 27 there is not significant difference between the mean square error introduced by quantization of a uniform or a gaussian density function. If we assume that the standard deviations of most of the input distributions to the quantizer in the TM system are in the range of .5 to 27, and the mean values are not near one of the edges of the quantizer, then it is a good approximation to use $\frac{\Delta^2}{12}$ as the mean square error introduced by the quantization operation.

By increasing the number of levels, making Δ smaller, we can make the mean square error as small as we want. In practice this can not be achieved because storage and bandwidth requirements impose an upper bound into the number of quantization levels actually used.

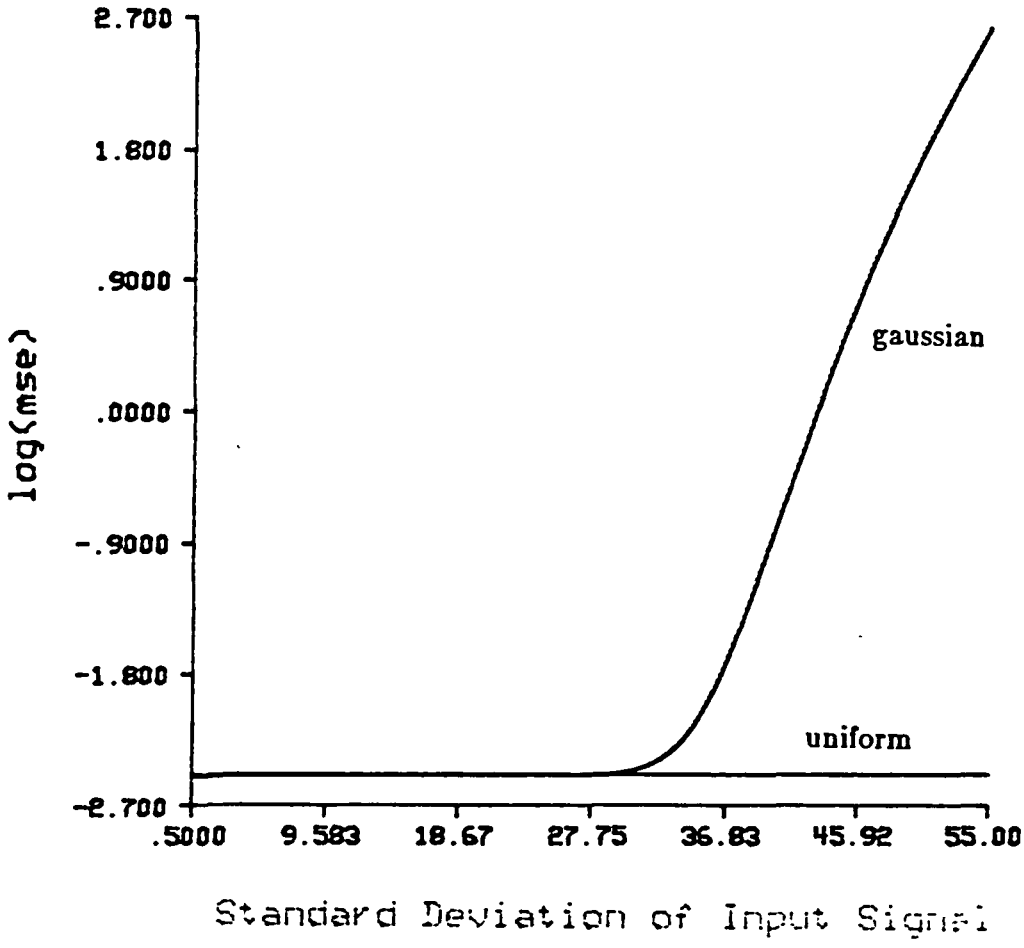

Figure 2.3 Mean square error at the output of an eight bit uniform quantizer for input signals that are uniformly and gaussianly distributed.

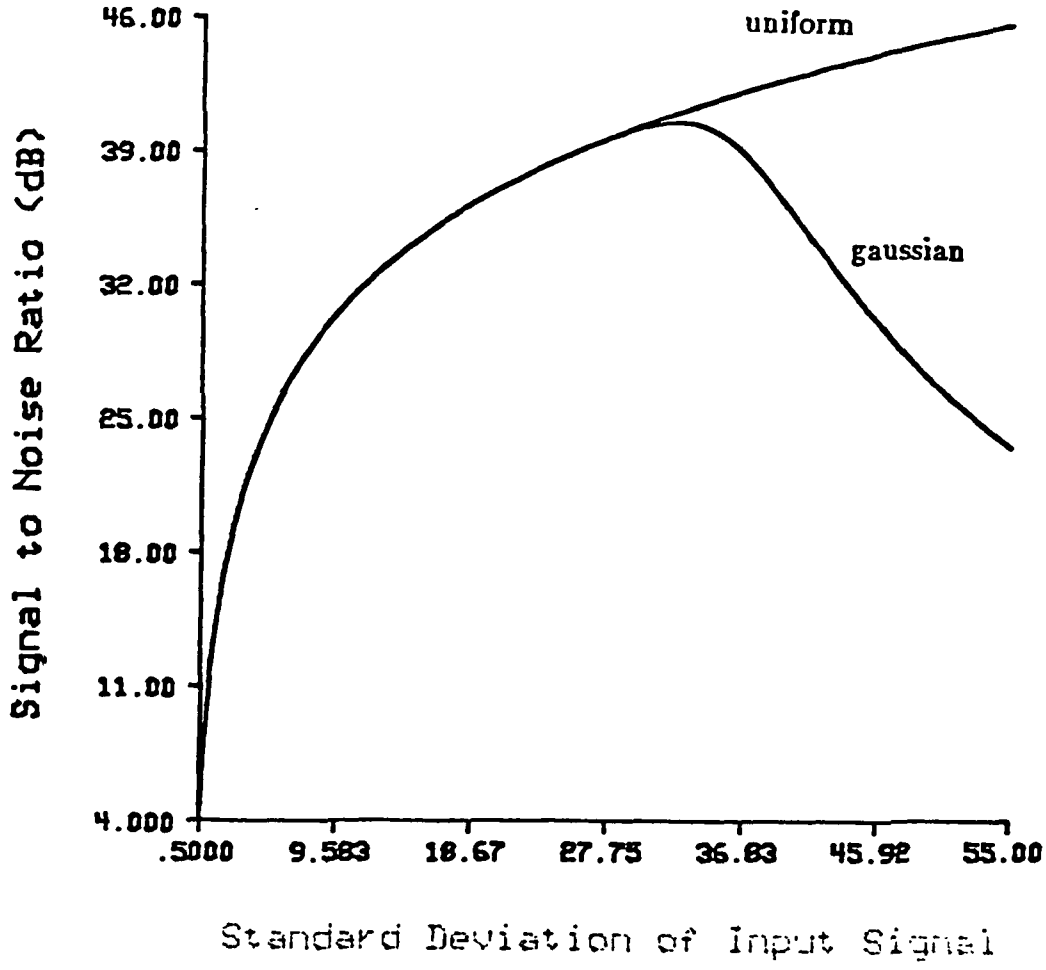

Figure 2.4 Signal-to-Noise Ratio at the output of an eight bit uniform quantizer for input signals that are uniformly and gaussianly distributed.

2.5 Johnson Noise

Johnson noise , also known as thermal noise, is produced by the random motion of electrons in a conductive material. In 1924, Johnson performed a systematic observation of the thermal fluctuations of electricity in conductors. His observations were in complete agreement with the predictions done by the theory of thermodynamics and quantum mechanics. The theory predicts [G2] that the mean square voltage produced in a resistor R is given by

$$\overline{(v-v_m)^2} = 4R(f)\frac{hf}{e^{\frac{hf}{kT}}-1}\Delta f, \tag{2.30}$$

where: h = Planck's constant, k = Boltzmann's constant, v is the instantaneous voltage, T is the temperature in degrees Kelvin, Δf is the bandwidth of the noise, and v_m is the mean voltage.

Thermal noise, black body radiation, and quantum noise can be developed from a few basic physical principles, as it was presented in a review paper by Oliver [O1]. The voltage induced by thermal noise has been shown to have a normal distribution with zero mean and variance kTBR.

$$p(v) = \frac{1}{\sqrt{2\pi kTBR}}\exp(-\frac{v^2}{2kTBR}), \tag{2.32}$$

where B is the bandwidth of the noise . This result could be expected on the basis of the Central Limit Theorem, because the voltage generated in an electrical circuit by the thermal noise is the summation of individual short

current pulses produced by the electrons in the conductive material as they travel between collisions. For practical purposes it can be assumed that the thermal noise is white since the electron pulses produced by the collisions are extremely short in duration. Thermal noise is also observed in lossy dielectrics as the result of random thermal excitations of polarizable molecules, forming fluctuating dipoles.

CHAPTER 3

MATHEMATICAL AND SOFTWARE MODEL

3.1 Description of the Model

In chapter two a statistical description of the noises in the Priority 1 list was presented. It is the purpose of this section to merge all of them together in a system that models the physical process of noise being added at different stages of the data acquisition process. In Fig. 3.1 a block diagram of the data acquisition system is shown, where all the noises are being referred to the radiance domain. This was done in order to avoid working with different types of units. We are not considering in this work the effects of the optics system in the signal. In vector equation form the model is described by

$$\mathbf{Z} = \mathbf{X}(\mathbf{L}) + \mathbf{U} + \mathbf{V}, \tag{3.1}$$

where, **X**, **U**, and **V** are independent random vectors.

Z - is the sensor output, which is the signal to be transmitted to earth.

L - is the radiance that gets into the sensor pupil after going through the atmosphere,

$$\mathbf{L} = \tau_a \mathbf{L}_s + \mathbf{L}_p.$$

X - is the photodetector output, it is a function of the signal level,

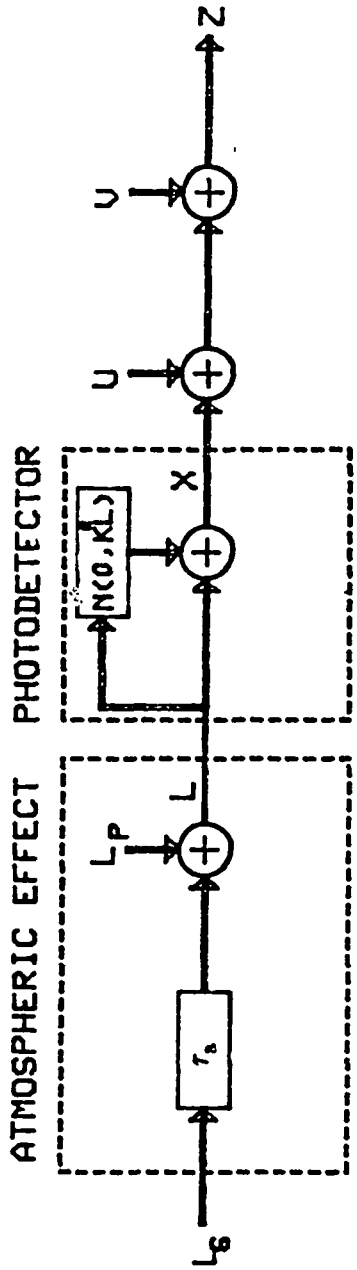

Figure 3.1 Block diagram of data acquisition system

$$\mathbf{X}(\mathbf{L}_s) = (\tau_a \mathbf{L}_s + \mathbf{L}_p) + N(0, K\sqrt{\tau_a \mathbf{L}_s + \mathbf{L}_p}).$$

U - preamp noise, is modeled by a gaussian distribution with zero mean and diagonal covariance matrix.

V - quantization noise, it is uniformly distributed with zero mean and $\Sigma_v = \frac{\Delta^2}{12}\mathbf{I}$, where Δ is the radiance range of one quantum level and **I** is the identity matrix.

The statistical properties of the input random process are modified at the different system stages. If we want to investigate the relationship between sensor parameters and overall performance we require a theoretical understanding of how the signal statistics are modified as it flows through the system. Although **X(L)** and **V** are not normally distributed, **Z** has been shown empirically [F3] to resemble a normal distribution. Arguments like the Central Limit Theorem are commonly used to substantiate this result. Since a multivariate gaussian distribution is completely specified by its covariance matrix and mean vector, we are interested to see how these random process parameters are affected by the system transformations. Another important descriptor to be considered, for each spectral band, is the correlation coefficient between the input and the output as a function of the system parameters.

In Fig. 3.1 **L** is the actual radiance vector that enters the sensor pupil and **X** is the photodetector output vector in the radiance domain. As was shown in chapter 2 the density function of a single photodetector output can be approximated by (3.2) as the number of electrons emitted in the interval $(0,\tau_h)$ becomes large,

$$p(\mathbf{X}_i|\,\mathbf{L}_i) = \frac{1}{\sqrt{2\pi k_i^2 \mathbf{L}_i}} \exp[\frac{-(\mathbf{X}_i-\mathbf{L}_i)^2}{2k_i^2\mathbf{L}_i}]. \tag{3.2}$$

k_i is a parameter descriptive of the photodetector performance and it is related to the system parameters discussed in the shot noise section of chapter two by $k_i^2 = \frac{T}{\tau_h \gamma}$. The correlation coefficient between $\mathbf{X}_i$ and $\mathbf{L}_i$ is given by

$$\rho_{X_i L_i} = \frac{E(\mathbf{X}_i\mathbf{L}_i) - E(\mathbf{L}_i)E(\mathbf{X}_i)}{\sigma_{X_i}\sigma_{L_i}}, \tag{3.3}$$

where,

$$E(\mathbf{X}_i) = E_{L_i}[E_{X_i}(\mathbf{X}_i|\,\mathbf{L}_i)] = E(\mathbf{L}_i) = \overline{L_i} \tag{3.4}$$

$$E(\mathbf{X}_i^2) = E_{L_i}[E_{X_i}(\mathbf{X}_i^2|\,\mathbf{L}_i)] = E(k_i^2\mathbf{L}_i + \mathbf{L}_i^2) = k_i^2\overline{L_i} + \overline{L_i^2} \tag{3.5}$$

$$\sigma_{X_i}^2 = E(\mathbf{X}_i^2) - E(\mathbf{X}_i)^2 = k_i^2\overline{L_i} + \sigma_{L_i}^2 \tag{3.6}$$

$$E(\mathbf{X}_i\mathbf{L}_i) = \int_{-\infty}^{\infty}\int \mathbf{X}_i\mathbf{L}_i p(\mathbf{X}_i|\,\mathbf{L}_i)p(\mathbf{L}_i)d\mathbf{X}_i d\mathbf{L}_i = E(\mathbf{L}_i^2) = \overline{L_i^2}. \tag{3.7}$$

So, $\rho_{X_i L_i}$ is equal to

$$\rho_{X_i L_i} = \frac{\sigma_{L_i}}{\sigma_{X_i}} = \frac{\sigma_{L_i}}{\sqrt{k_i^2 \overline{L_i} + \sigma_{L_i}^2}}. \tag{3.8}$$

This is a general result and does not rely on the asymptotic condition imposed over the shot noise process to obtain (3.2). Observe, $\rho_{X_i L_i}$ is approximately equal to one if $k_i^2 \ll \frac{\sigma_{L_i}^2}{\overline{L_i}}$; this will correspond to an ideal photodetector. For a single spectral band the input-output correlation is

$$\rho_{Z_i L_i} = \frac{E(Z_i L_i) - E(Z_i)E(L_i)}{\sigma_{Z_i}\sigma_{L_i}}. \tag{3.9}$$

Since X_i, U_i, and V_i are independent random variables

$$\sigma_{Z_i}^2 = \sigma_{X_i}^2 + \sigma_{U_i}^2 + \sigma_{V_i}^2 \tag{3.10}$$

$$E(z) = \overline{L_i}$$

$$E(Z_i L_i) = E(L_i(X_i + U_i + V_i)) = E(L_i X_i) = \overline{L_i^2}.$$

So,

$$\rho_{Z_i L_i} = \frac{\sigma_{L_i}}{\sigma_{Z_i}}. \tag{3.11.a}$$

Using the atmospheric model discussed in chapter two, $L_i = \tau_a L_{si} + L_p$, the

correlation coefficient between the input signal $\mathbf{L}_{si}$ and $\mathbf{Z}_i$ for a given spectral band is

$$\rho_{Z_i L_{si}} = \frac{\tau_a \sigma_{L_{si}}}{\sqrt{\tau_a^2 \sigma_{L_{si}}^2 + k_i^2(\tau_a \overline{L_{si}} + L_p) + \sigma_{U_i}^2 + \sigma_{V_i}^2}} \tag{3.11.b}$$

As a test of the physical significance of (3.11.b) observe, for zero atmospheric transmittance $\rho_{Z_i L_{si}} = 0$, and for no system noise, $k_i = \sigma_{U_i} = \sigma_{V_i} = 0$, the correlation coefficient is equal to one. Equation (3.11.b) clearly shows that the magnitude of the input-output correlation in a particular spectral band goes down as the average input radiance of the signal in that spectral band increases.

For the definition of signal-to-noise ratio (SNR), using the variance of the signal, taken as $\tau_a^2 \sigma_{L_{si}}^2$, over the variance of the noise, $k_i^2(\tau_a \overline{L_{si}} + L_p) + \sigma_{U_i}^2 + \sigma_{V_i}^2$, we can express the SNR for each channel in terms of the input-output correlation as

$$\text{SNR} = \frac{\rho_{Z_i L_{si}}^2}{1 - \rho_{Z_i L_{si}}^2}. \tag{3.12}$$

Recalling $\mathbf{X}_i$, $\mathbf{U}_i$, and $\mathbf{V}_i$ are independent vectors we can state that the output covariance matrix is given by

$$\Sigma_z = \Sigma_x + \Sigma_u + \Sigma_v, \tag{3.13}$$

where the covariance matrix for $\mathbf{U}$ and $\mathbf{V}$ are diagonal matrices that are specified by system parameters. Σ_x is formed by diagonal elements $\sigma_{x_i}^2$, (3.6) ,

and off diagonal elements $\rho_{x_i x_j}\sigma_{x_i}\sigma_{x_j}$ where ,

$$\rho_{X_iX_j} = \frac{E(X_iX_j)-\overline{X_i}\,\overline{X_j}}{\sigma_{X_i}\sigma_{X_j}} \tag{3.14}$$

$$\overline{X_i} = \overline{L_i} \quad \text{and} \quad \sigma_{X_i}^2 = k_i^2\overline{L_i}+\sigma_{L_i}^2.$$

Using the model adopted in chapter two for a photodetector output, we have

$$\mathbf{X}_i(\mathbf{L}_i) = \mathbf{L}_i + N(0,k_i\sqrt{\mathbf{L}_i}), \tag{3.15}$$

where the i^{th} channel output is equal to the input radiance $\mathbf{L}_i$ plus a random variable with zero mean and variance $k_i^2\mathbf{L}_i$. An expression for the cross spectral output correlation, $\rho_{X_iX_j}$, can be obtained from,

$$E(\mathbf{X}_i\mathbf{X}_j) = E[(\mathbf{L}_i+n_i)(\mathbf{L}_j+n_j)] = E(\mathbf{L}_i\mathbf{L}_j)$$

so,

$$\rho_{X_iX_j} = \frac{E(\mathbf{L}_i\mathbf{L}_j)-\overline{L_i}\,\overline{L_j}}{\sigma_{X_i}\sigma_{X_j}} = \rho_{L_iL_j}\left[\frac{\sigma_{L_i}\sigma_{L_j}}{\sigma_{X_i}\sigma_{X_j}}\right]. \tag{3.16}$$

This is an interesting expression because it allows us to describe the photodetector output cross spectral correlation in terms of the input cross spectral correlation, $\rho_{L_iL_j}$. Combining (3.13) and (3.16) an expression for the output covariance matrix and mean vector can be obtained in terms of the different system noise sources,

$$E[\mathbf{Z}] = E[\mathbf{L}] = \tau_a E[\mathbf{L}_s] + L_{eq}(I-\tau_a) \tag{3.17}$$

$$\Sigma_z = \begin{bmatrix} \sigma_{L_1}^2 + k_1^2\overline{L_1} + \sigma_{U_1}^2 + \sigma_{V_1}^2 & & & \\ \rho_{L_1L_2}\sigma_{L_1}\sigma_{L_2} & \sigma_{L_2}^2 + k_2\overline{L_2} + \sigma_{U_2}^2 + \sigma_{V_2}^2 & & \\ \vdots & \vdots & \ddots & \\ \rho_{L_1L_n}\sigma_{L_1}\sigma_{L_n} & \rho_{L_2L_n}\sigma_{L_2}\sigma_{L_n} & & \sigma_{L_n}^2 + k_n\overline{L_n} + \sigma_{U_n}^2 + \sigma_{V_n}^2 \end{bmatrix} \tag{3.18}$$

Since a covariance matrix is a symmetric matrix the upper diagonal elements in (3.18) were omitted. Observe that the off diagonal elements of Σ_z are equal to the off diagonal elements of Σ_l. This implies a smaller correlation coefficient between spectral bands at the output of the system, because the expression inside the brackets in (3.19) is less than one.

$$\rho_{Z_iZ_j} = \rho_{L_iL_j}\left[\frac{\sigma_{L_i}\sigma_{L_j}}{\sqrt{(\sigma_{L_i}^2 + k_i^2\overline{L_i} + \sigma_{U_i}^2 + \sigma_{V_i}^2)(\sigma_{L_j}^2 + k_j^2\overline{L_j} + \sigma_{U_j}^2 + \sigma_{V_j}^2)}}\right] \tag{3.19}$$

Summarizing, in this section an additive noise model has been adopted to describe the relationship between system parameters and the signal, and the output covariance matrix of this model was computed. It was shown that the higher the average radiance in a particular spectral band the lower the correlation between the input and the output of the system. Equations (3.11), (3.12), (3.17) and, (3.18) can be used in the evaluation or design phase of system parameters if statistical knowledge of the different kinds of signals to be observed is available. Having an analytical expression for the output

covariance matrices and the input-output correlation allows us to use parametric statistical pattern recognition techniques for the study of system parameters without having to actually generate the data sets representative of the noisy signal.

3.2 Index of Performance

If one is interested in the evaluation or design of system parameters a variable or variables against which any given parameter set can be compared is needed. Probability of correct classification or its complement the probability of error is a good choice for such an index of performance from a user point of view. Unfortunately, the Bayes minimum error can not be expressed in an analytical form because it involves a multidimensional integration over a complex boundary region,

$$\epsilon = 1 - \sum_{i=1}^{n} P(w_i) \int_{\Gamma_i} p(\mathbf{Z} | w_i) dZ. \tag{3.20}$$

$P(w_i)$ is the a priori probability of class w_i , $p(Z | w_i)$ is the density function of Z given that Z comes from class w_i, and Γ_i is the region in the multidimensional space where the Bayes criteria has classified the samples into class w_i.

There are different algorithms which are commonly used for the error estimation. For example, random sampling techniques, such as Monte Carlo simulations, can be used for estimating the error. In this scheme, N random vectors are generated from the training samples statistics and they are

classified in accordance to the Bayes decision criteria. The number of incorrectly classified samples divided by N gives the maximum likelihood estimate of the Bayes error. This estimator is known to be unbiased [F1]. The error estimation to be obtained from a Monte Carlo simulation is a random variable which is dependent on the number of samples used. For accurate estimates a large number of samples are required which implies large amounts of CPU time. An algorithm was presented by Fukunaga and Krile [F2], for a two class problem, which transforms the multidimensional integration of (3.20) into a one dimensional integration in the frequency domain. This algorithm, in theory, is exact. Although, small errors may be introduced by its numerical implementation, compared to Monte Carlo simulations, it is more accurate, and more efficient in machine time.

Statistical separability can be used as an alternative index of performance when the probability of error results are inconvenient to compute. A well known statistical distance function between two gaussianly distributed classes is the Bhattacharyya distance[B1],

$$\mu = \frac{1}{8}(M_1-M_2)^T[\frac{\Sigma_1+\Sigma_2}{2}]^{-1}(M_1-M_2)+\frac{1}{2}\ln\frac{|\frac{1}{2}(\Sigma_1+\Sigma_2)|}{|\Sigma_1|^{\frac{1}{2}}|\Sigma_2|^{\frac{1}{2}}} \qquad (3.21)$$

which has been commonly used for feature extraction applications [S3]. It is appealing to use the Bhattacharyya distance as an aid in the design or evaluation of system parameter. Although, there is not an exact relationship between probability of error and the Bhattacharyya distance, an upper and a lower bound exists for the Bayes error in terms of μ [F1],

$$\frac{1}{2}[1-\sqrt{1-4\epsilon_u{}^2}] \leq \epsilon \leq \epsilon_u = \frac{1}{2}e^{-\mu}. \tag{3.22}$$

Based on simulation results Whitsitt [W1] suggested the usage of the complementary error function of $\sqrt{2\mu}$ as an approximation of the Bayes error. When the two classes under consideration have equal covariance matrices and equal a priori probabilities, the approximation turns into an equality. If this is a good approximation it has to be bounded between the upper and the lower bound of the Bayes error, given by (3.22), for all values of μ. A proof of the consistency of this approximation follows.

The complementary error function is defined as

$$Q(x) = \int_x^\infty \frac{1}{\sqrt{2\pi}} e^{\frac{-x^2}{2}} dx. \tag{3.23}$$

It is known Q(x) has an upper bound given by [V1],

$$Q(x) \leq \frac{1}{2} e^{-\frac{x^2}{2}} \quad x \geq 0. \tag{3.24}$$

Replacing x by $\sqrt{2\mu}$ in (3.24) it is easily proved $Q(\sqrt{2\mu})$ is less than the upper bound given by (3.22). The lower bound consistency can be proven by putting the left hand side of (3.22) in the form

$$1 \leq 2Q(\sqrt{2\mu}) + \sqrt{1-e^{-2\mu}} = g(\mu). \tag{3.25}$$

Observe that at μ equal zero or infinity the equality is satisfied. Since $g(\mu)$ has

these boundary conditions, if it ever goes below the value one, it will have a minimum point. Taking the derivative of $g(\mu)$, using the Leibnitz rule of derivation under the integral sign, and setting it equal to zero, we obtain

$$g'(\mu) = \frac{-2}{\sqrt{2\pi}} e^{-\mu}(2\mu)^{\frac{-1}{2}} + e^{-2\mu}(1-e^{-2\mu})^{\frac{-1}{2}} = 0.$$

Since we are interested in the relative minimum in the open interval $(0,\infty)$ the previous expression can be simplified into

$$e^{-2\mu}[\pi\mu + 1] = 1,$$

which can be solved interactively obtaining the value $\mu = .4221$. Substituing this value in (3.25) we obtain

$$1 \leq g(.4221) = 1.113 .$$

This proves the approximation is consistent with the bounds established on the Bayes error by (3.22). The advantage of using $Q(\sqrt{2\mu})$ as an approximation of the Bayes error is that it does not require extensive computer computations. In Fig. 3.2 the relationship between $Q(\sqrt{2\mu})$ and the upper and lower bounds on the error probability is shown.

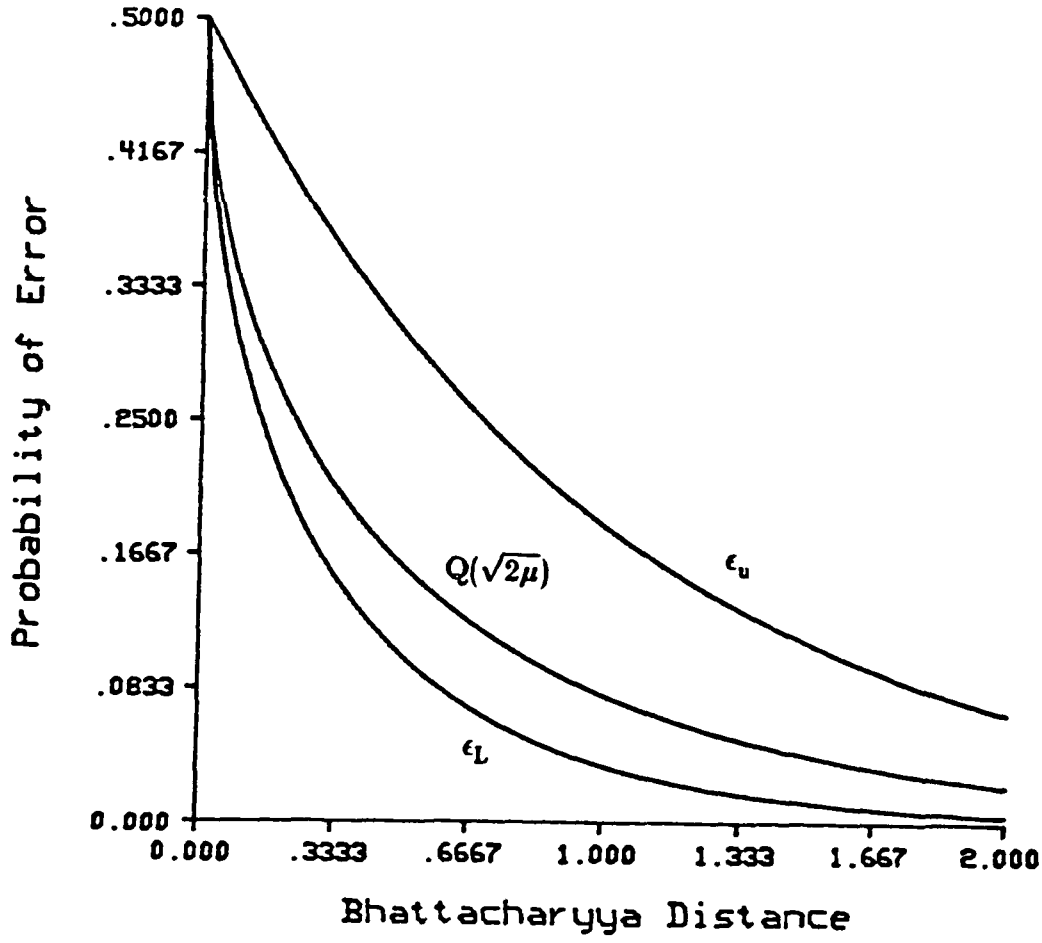

Figure 3.2 Comparison of the upper bound, lower bound and approximating function of the Bayes error obtained from the Bhattacharyya distance.

3.3 Software System

The next step was to construct a software system which could adequately simulate noise from each of the types of sources to be considered. In order to simplify the problem, only two classes with equal a priori probabilities were simultaneously considered, and the output distribution of these was assume to be gaussian. Since real data is likely to have characteristics that are highly dependent on outside and uncontrollable elements, such as deviations from the gaussian assumption, it was decided to use the covariance matrices obtained *from training samples as the input signal.* Thus a system of computer programs was written to allow for the use of a LARSYS data statistics file as input and to use it to simulate an unadulterated signal source. In general the required inputs to the software system are:

1- Atmospheric optical thickness vector and solar zenith angle

2- Duntley's equivalent radiance vector, L_{eq}

3- k vector, with shot noise system parameters

4- Covariance matrices for preamp and quantization noise

5- Spectral covariance matrices and mean vectors for the two classes to be considered

6- Weighting factors vector for the selective adjustment of the different noise sources

The software output consists of:

1- Bayes minimum error for each output class and overall

2- Bhattacharyya distance between two output classes

3- Complementary error function of $\sqrt{2\mu}$

For computing the pairwise error, the algorithm developed by Fukunaga and

Krile was used. A list of the software programs can be found in Appendix C.

3.4 Selection of the Data Set

As an initial data set airborne multispectral scanner data of Segment 210 of the 1971 Corn Blight Watch Experiment was selected. The scanner instrument used to collect this data was the Michigan M-7 airborne scanner. The selection of this data set was influenced by the following factors:

1- Ground truth for every pixel should be available. This is important both for deriving good quality training samples and for accurate determination of performance.

2- The characteristics for this data set, e.g. the number of spectral bands and the ground spatial resolution, are representative of possible future spaceborne scanners.

3- The informational classes in the ground scene are adequately complex to be representative of possible future applications and to provide a significant challenge against which to test future scanner system designs. Out of this data set we used a subset of classes that gave good classification performance when no noise was present, but was sensitive to the noise levels introduced by the sensor system. The criteria adopted to choose these classes was based on the coincidental spectral plot from the training samples of segment 210 .

It was decided to use bands and noise levels which approximate the Thematic Mapper in order to enhance the practical benefits of the study. Channels 1,5,7,8,10 from segment 210 data were the ones which had the best

match with channels 1,2,3,4,5 in the Thematic Mapper. The Thematic Mapper noise equivalent radiance curves for quantization, preamp, and shot noise were obtained from NASA's Goddard Space Center for the first five spectral bands in the TM, see Figure 3.3 to 3.7. This curves clearly show the dependence between shot noise and the signal level.

3.5 Simulations Performed and Results

In this section it is shown how, by using the model developed, we can investigate the relationship between classification accuracy, sensor parameters, class statistics and the atmospheric effects. In particular, we want to study if by slightly adjusting the noise levels introduced by the Thematic Mapper sensor system we can make a significant change in the recognition accuracy. Another parameter to be modified is the atmospheric visibility.

A series of different computer simulations were conducted using the developed software system. In these runs the data set used came from the Corn Blight Watch experiment. We considered this data set as representative of a noise free data set and for the purpose of the simulation we assumed it was collected under perfect atmospheric conditions by an ideal TM kind of instrument. Using the software system we can corrupt the signal statistics, based on the chosen system parameters, and quantify the degradation in terms of the index of performance proposed in the previous sections.

In the first experimental run the inputs were:

1- Equivalent radiance vector, $L_{eq} = 150(1,1,1,1,1)^T$, the particular choice of this vector value was arbitrary.

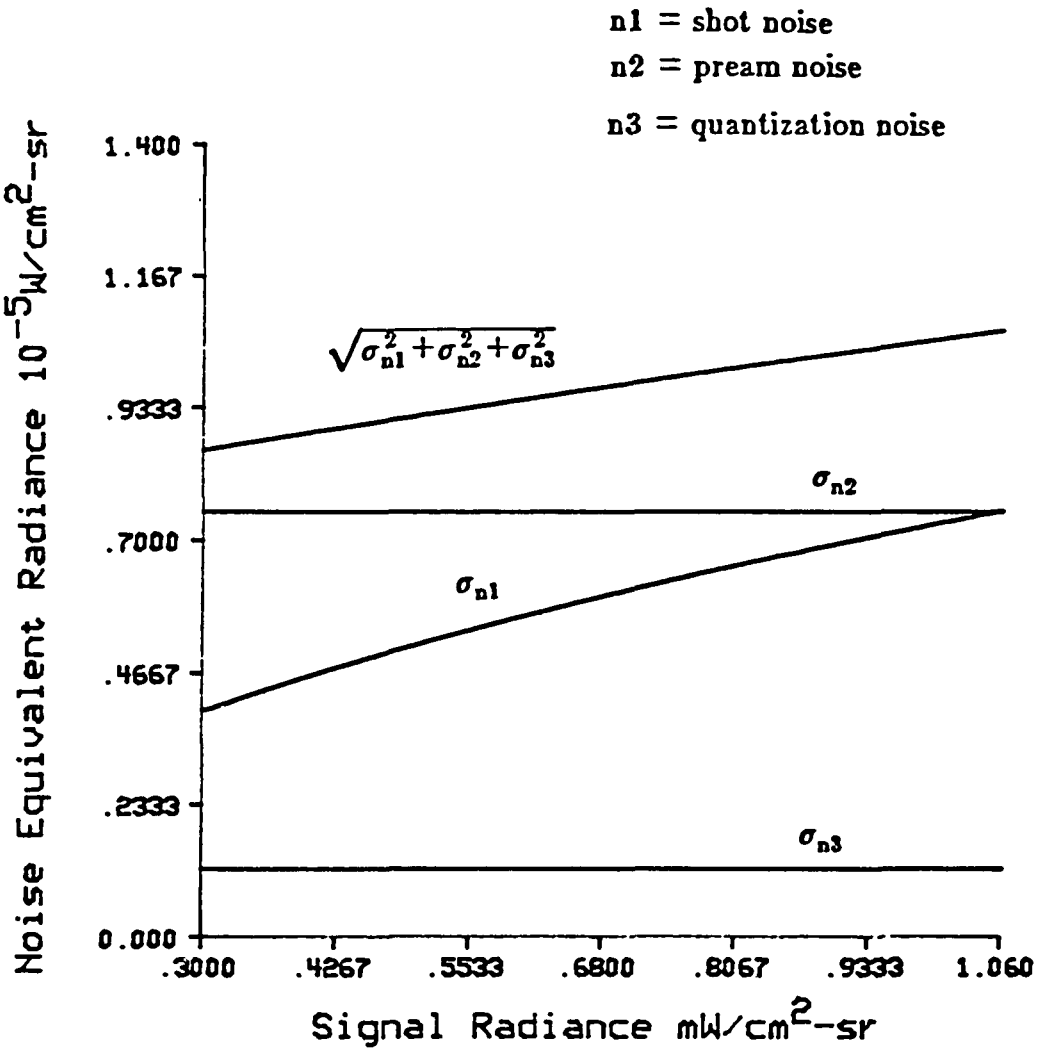

Figure 3.3 Thematic Mapper noise equivalent radiance in the .45 - .52 um band. Channel gain is set to have 1.06 mW/cm^2-sr = 256 bits.

n1 = shot noise
n2 = pream noise
n3 = quantization n

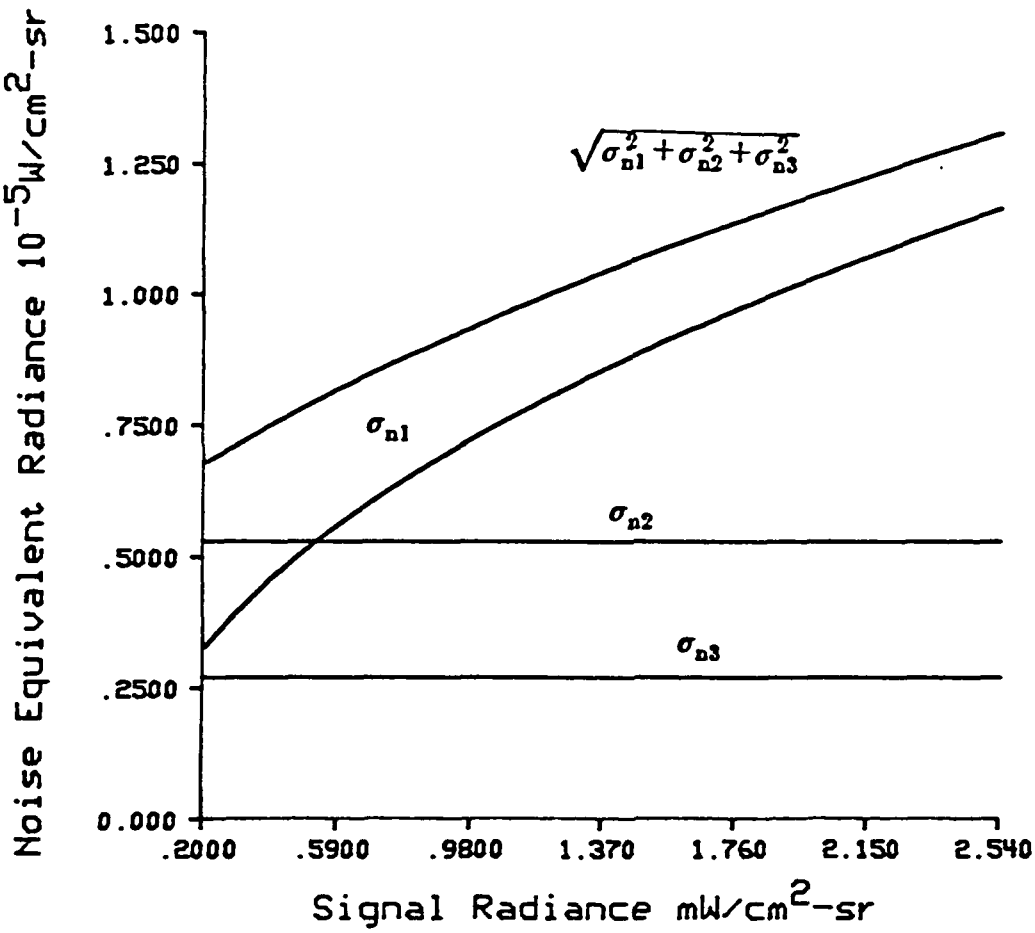

Figure 3.4 Thematic Mapper noise equivalent radiance in the .52 - .60 um band. Channel gain is set to have 2.54 mW/cm^2-sr = 256 bits.

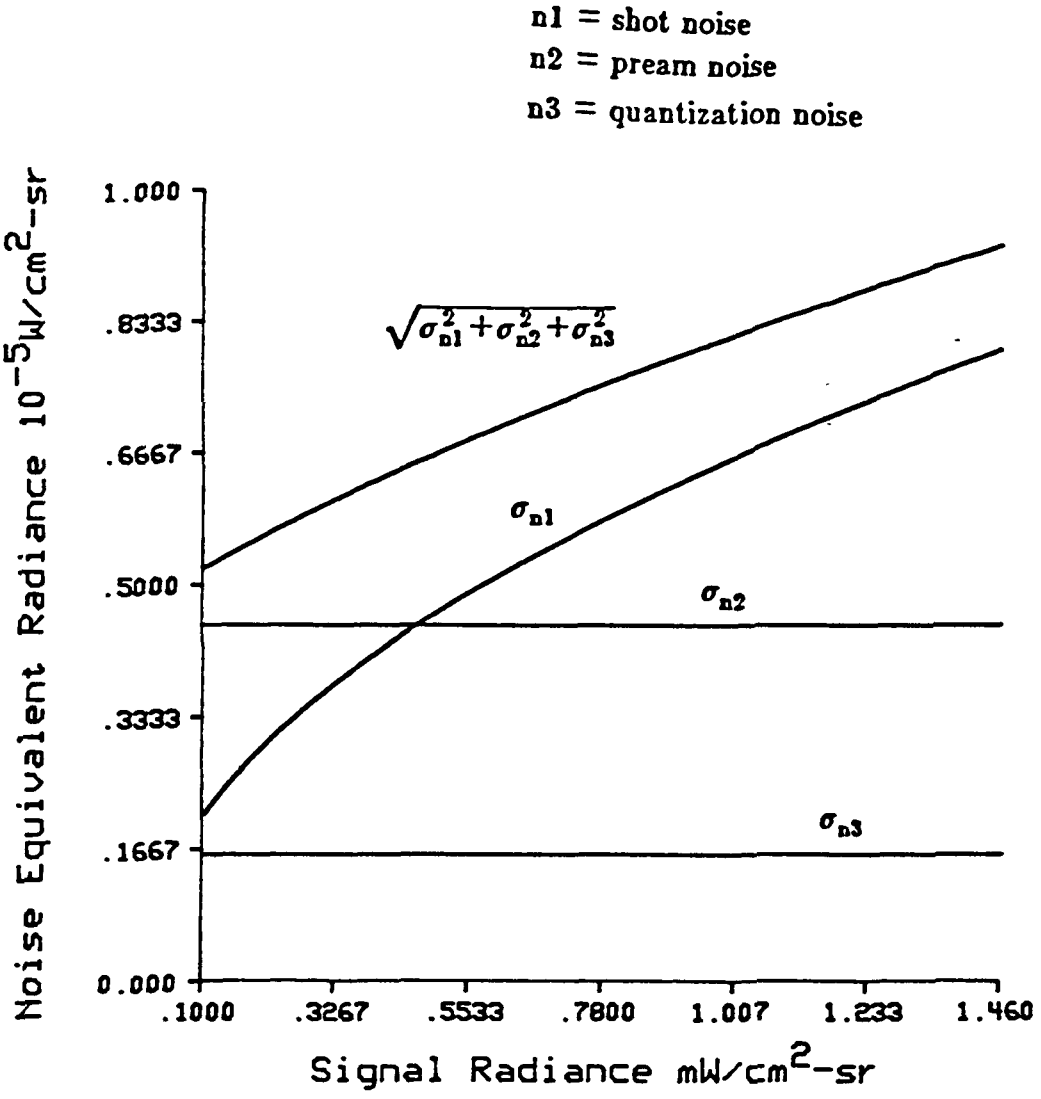

Figure 3.5 Thematic Mapper noise equivalent radiance in the .63 - .69 um band. Channel gain is set to have 1.46mW/cm^2-sr = 256bits.

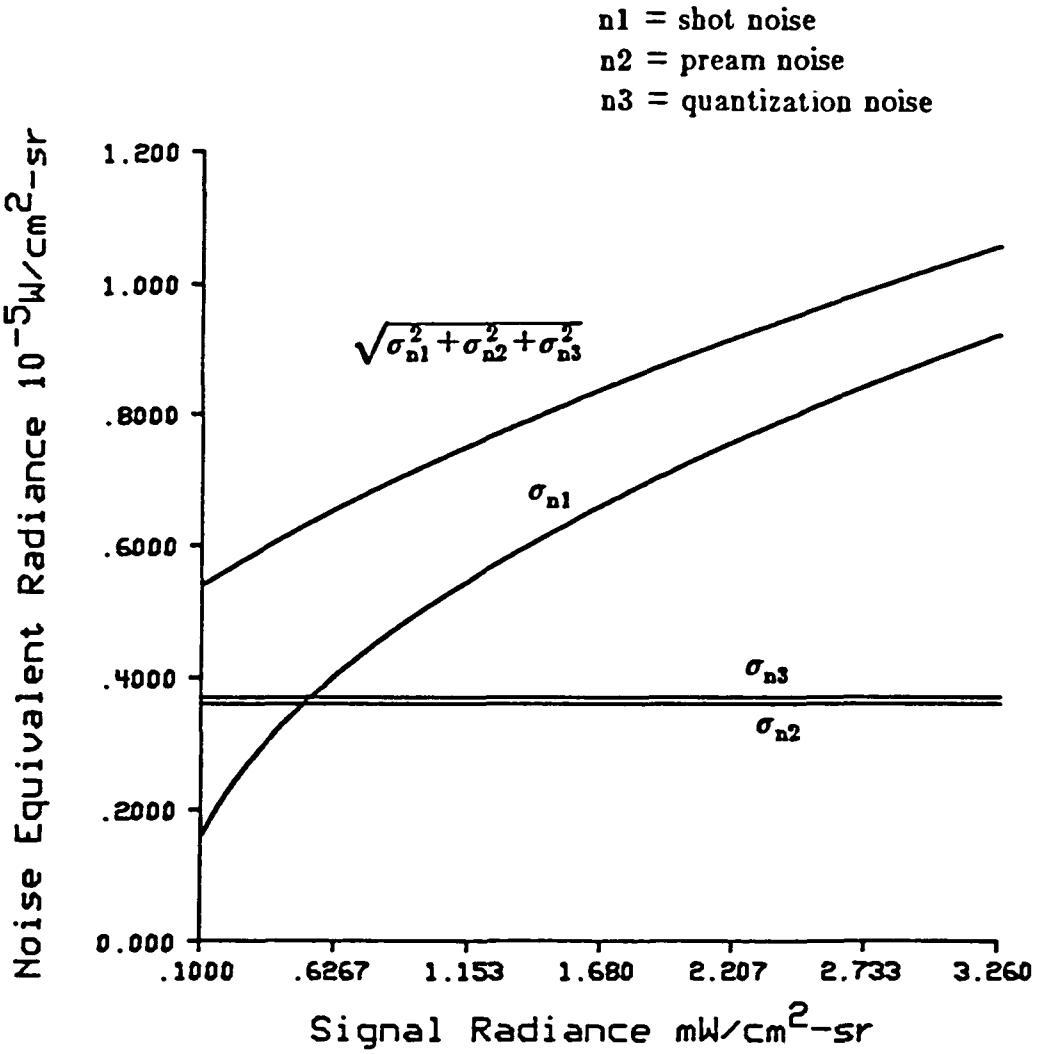

Figure 3.6 Thematic Mapper noise equivalent radiance in the .75 - .91 um band. Channel gain is set to have 3.26 mW/cm^2-sr = 256 bits.

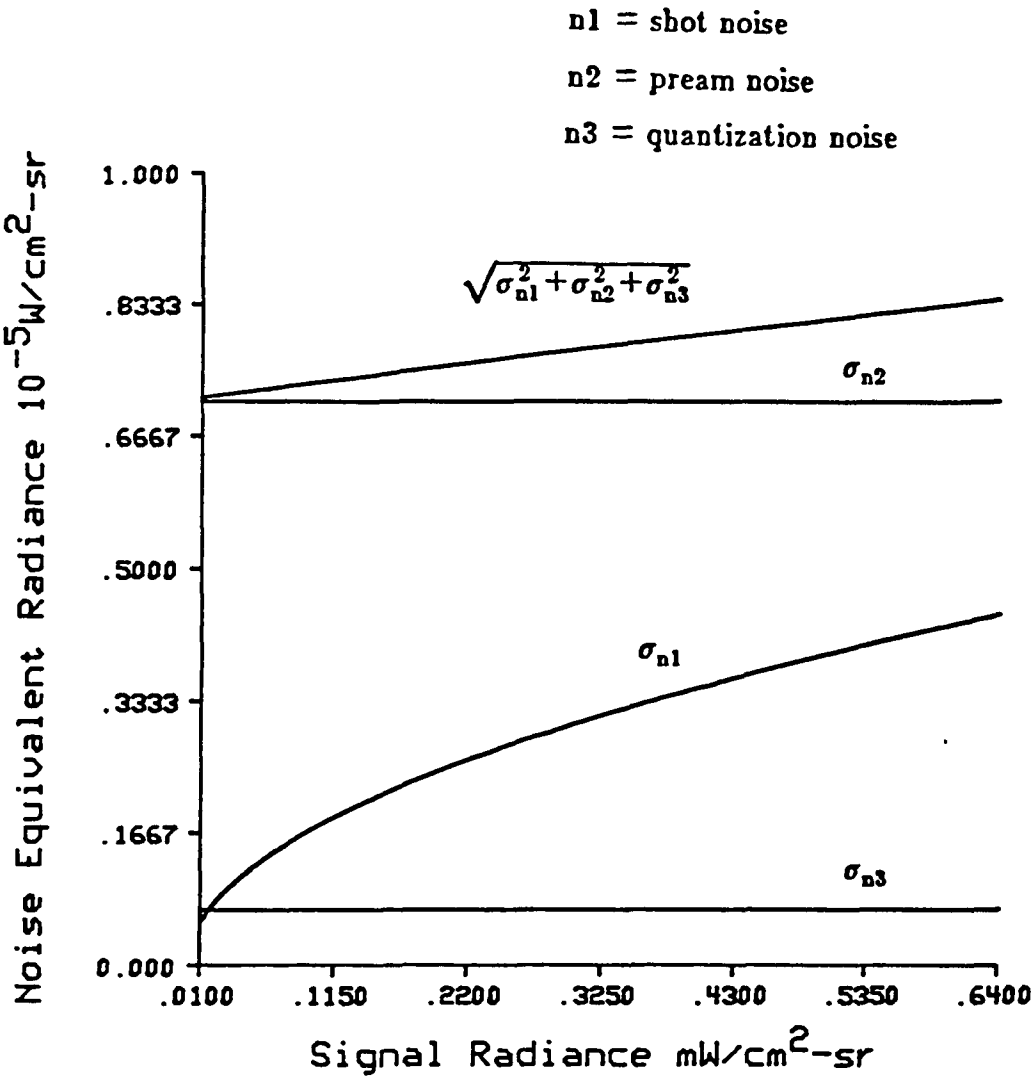

Figure 3.7 Thematic Mapper noise equivalent radiance in the 1.55 - 1.75 um band. Channel gain is set to have .64 mW/cm^2-sr = 256 bits.

2- Atmospheric optical thickness matrix for a haze atmosphere. Eight different metereological ranges were considered, see chapter two.

3- Thematic Mapper noise equivalent radiance system parameters for shot, preamp and quantization noise; this was obtained from NASA.

4- Covariance matrices and mean vectors for the two input classes, see Fig. 3.8. This matrices correspond to the subclasses soy1 and soy2 obtained from the training samples selected by LARS staff.

In Fig. 3.9 is shown the results of how the Bayes error changes for different atmospheric visibilities, which correspond to a haze regime. Observe that for high visibilities the error due to preamp noise alone is significantly larger than that due to shot noise and quantization noise. This is in complete agreement with the kind of theoretical result expected from (3.17) because the atmosphere attenuates the power in the signal and introduces a path radiance component into the signal. This causes the two input signals to approach one another making them more susceptible to system noise. Fig 3.10 shows that the same relative results would be obtained when $Q(\sqrt{2\mu})$ is considered, although the values of $Q(\sqrt{2\mu})$ are always least when compared to the values of the error. Figure 3.10 is a smoother version of Fig. 3.9; this is explained by the fact that the function $Q(\sqrt{2\mu})$ is an approximation of the actual error and can not track perfectly the fluctuations in it. Quantization noise did not show a significant variation in the recognition accuracy for the range of atmospheres considered and was the less degradating noise source in the system.

The results in Fig. 3.11 correspond to an atmosphere with a horizontal visibility of eight kilometers. Here it is shown how the Bayes error changes when the shot noise parameters, K, are adjusted by a variable c from zero times its original or actual value to twice its actual value. While this

$$M_1 = [120.98,114.74,81.96,144.39,162.24]^T$$

$$\Sigma_1 = \begin{bmatrix} 143.06 & & & & \\ 142.52 & 167.5 & & & \\ 179.29 & 209.13 & 276.90 & & \\ -19.62 & -34.3 & -51.5 & 66.5 & \\ 81.7 & 88.01 & 112.95 & 1.96 & 73.81 \end{bmatrix}$$

$$M_2 = [115.36,109.26,76.94,141.65,149.94]^T$$

$$\Sigma_2 = \begin{bmatrix} 16,8 & & & & \\ 5.11 & 13.94 & & & \\ 2.61 & 6.11 & 7.72 & & \\ -.99 & -3.06 & -4.83 & 25.5 & \\ -1.35 & -7.11 & -2.90 & 7.43 & 39.92 \end{bmatrix}$$

Figure 3.8 Statistics for subclasses soy 1 and soy 2.

parameter was changed the rest of the system parameters were set to their original values. There was a change of approximately five percent between the maximum and the minimum of the Bayes error in Fig. 3.11. Figure 3.12 shows the same type of result when the preamp noise level is the adjusted parameter.

In Figure 3.13, the adjusted system parameter was the number of bits used by the quantizer for representing the dynamical range of the incoming signals. When this result is compared to Fig. 3.9 it is observed that if five bits

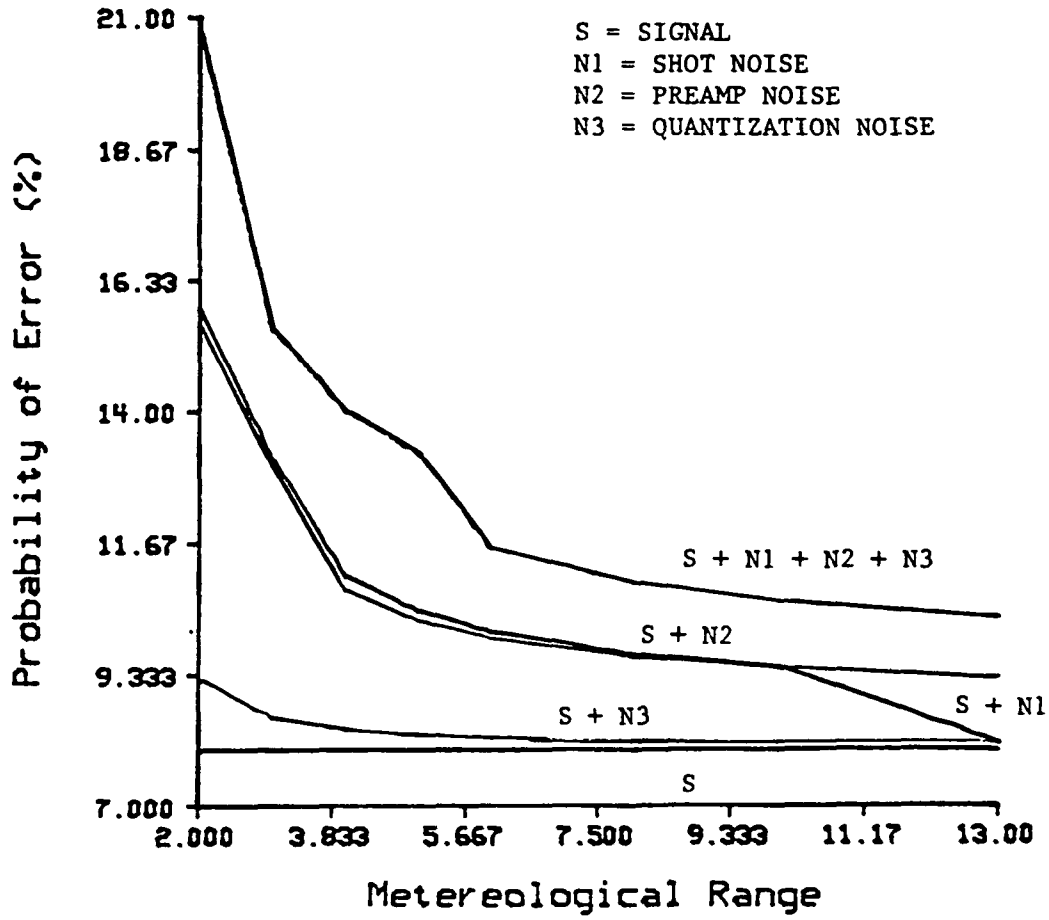

Figure 3.9 Probability of error versus metereological range.

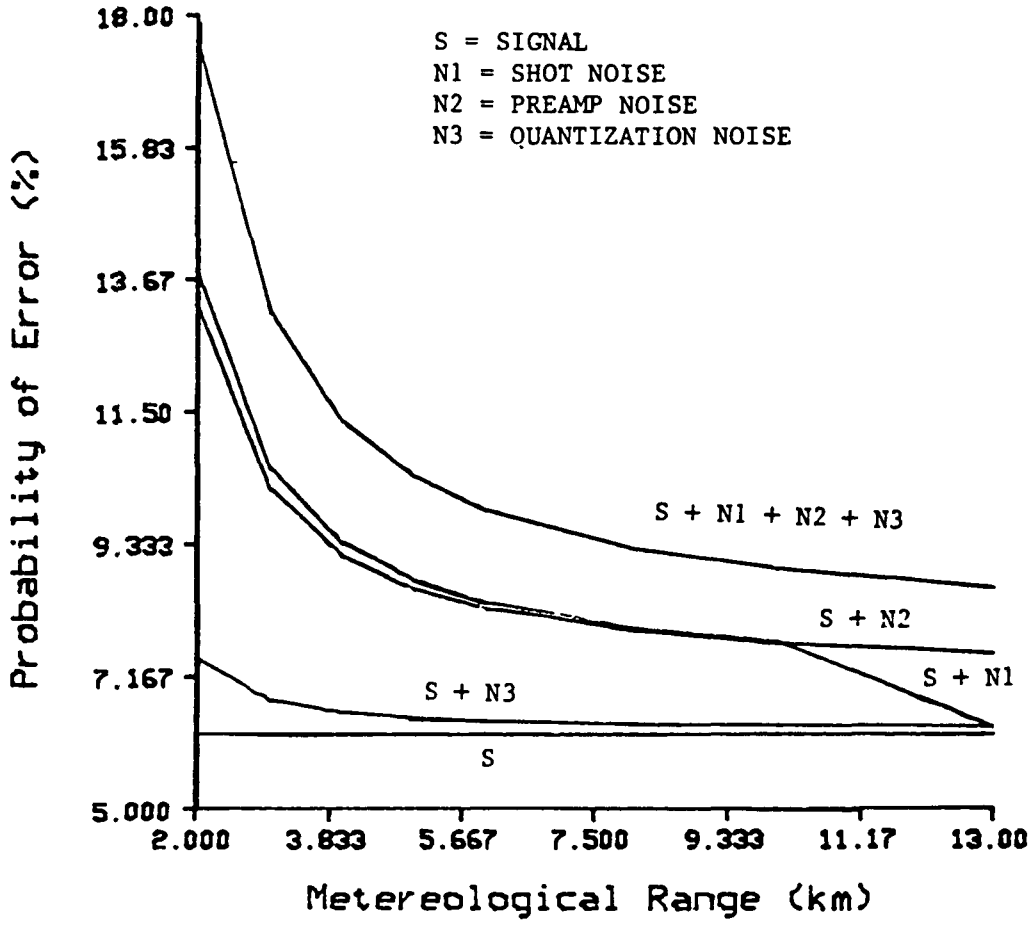

Figure 3.10 Bayes error approximating function versus metereological range.

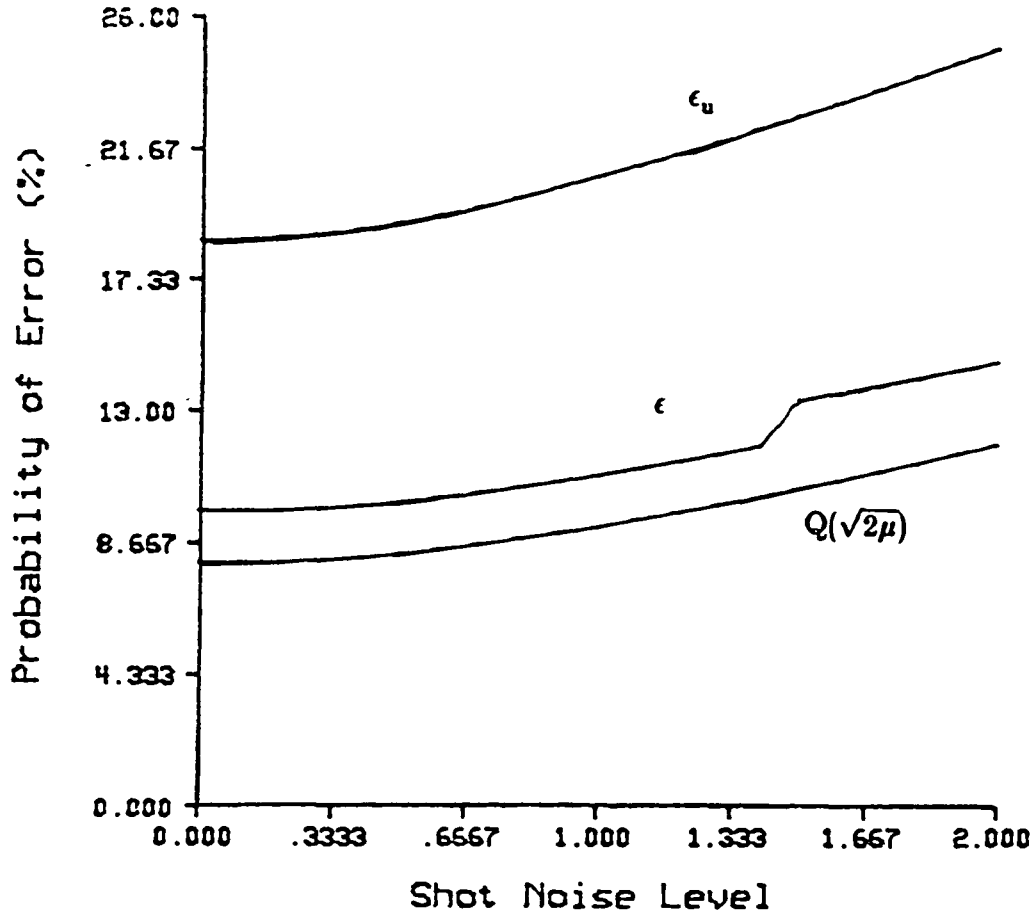

Figure 3.11 Probability of error versus shot noise level for an atmospheric metereological range of 8 km.

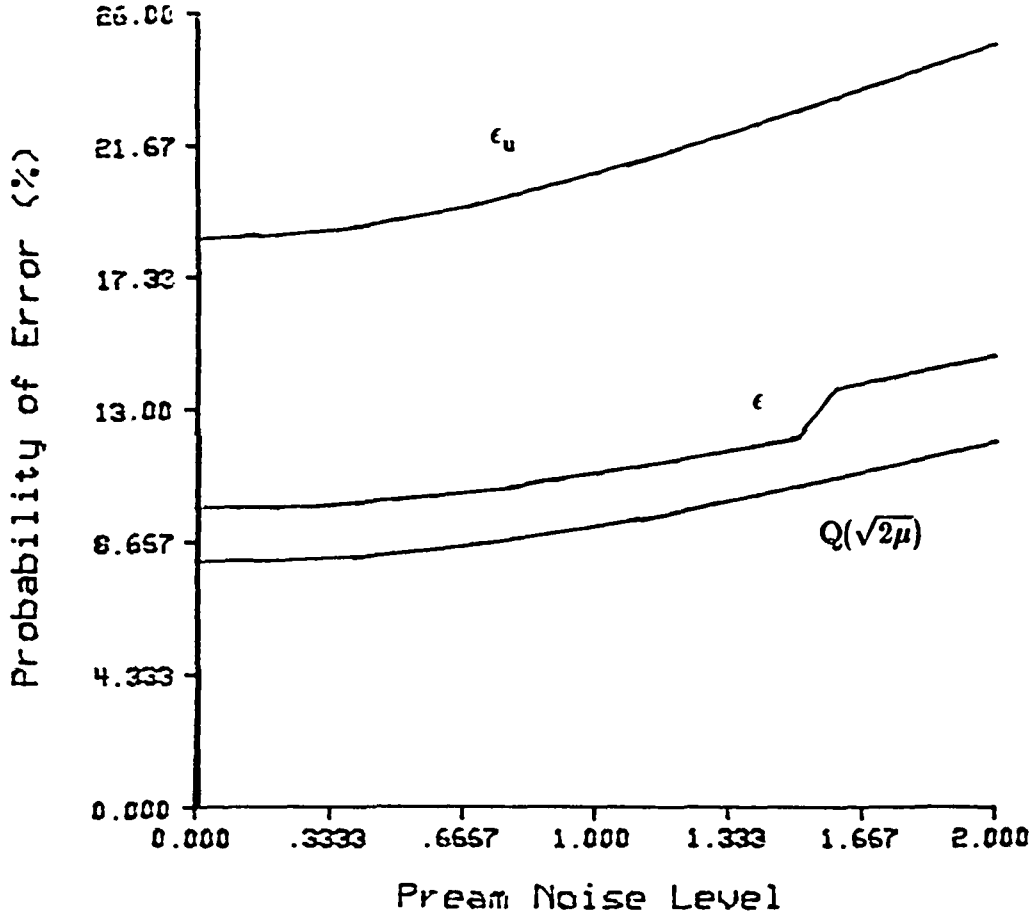

Figure 3.12 Probability of error versus preamp noise level for an atmospheric metereological range of 8 km.

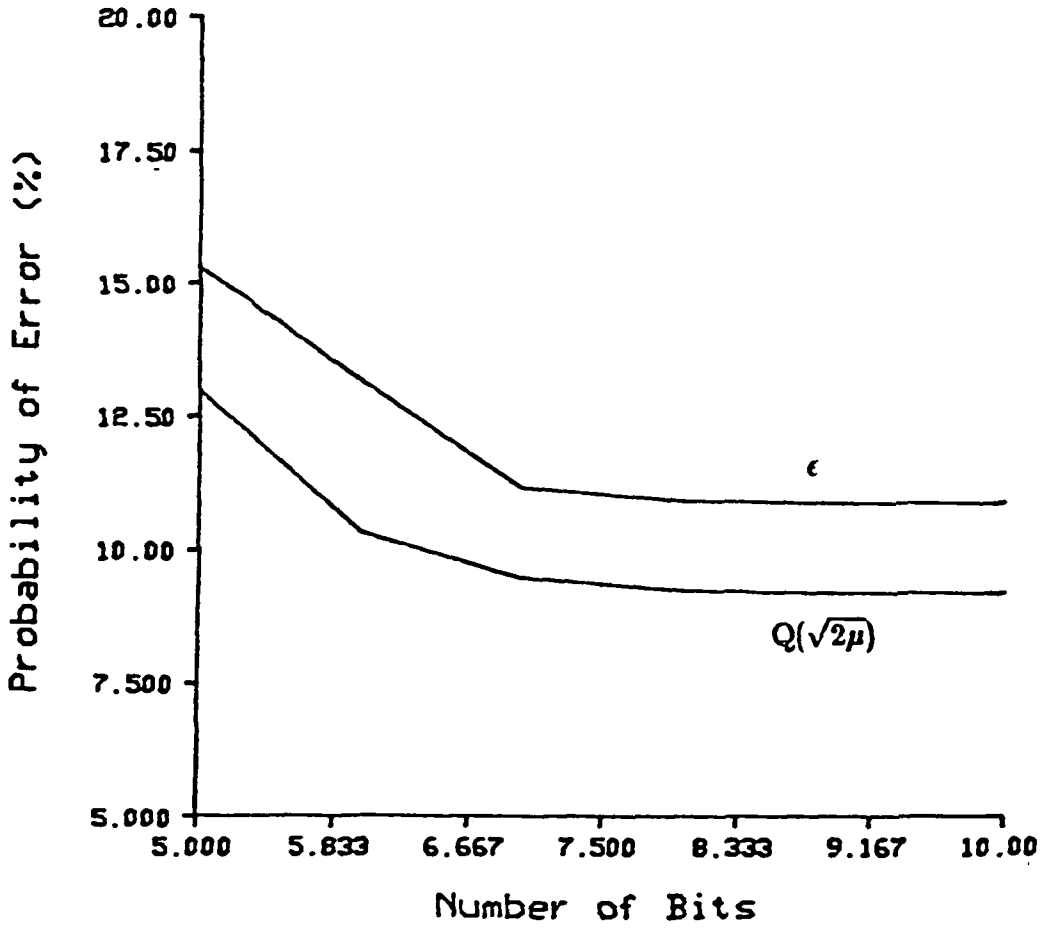

Figure 3.13 Probability of error versus number of bits used by the uniform quantizer.

were used, the quantization noise turns out to be the most predominant source of noise. For the particular set of classes considered in Fig. 3.13, an improvement in the number of bits from eight shows no significant difference in the probability of error.

The purpose of this section was to show how the software system could be used to evaluate the response of a multispectral scanner under different operational environments and different sensor parameters. The results obtained here were specific for the two input classes selected.

3.6 Removal of Atmospheric Effects and Noise

As was observed with regard to Fig. 3.9, the atmosphere has an important role in the degradation of class recognition. Based on the noise free atmospheric model discussed in Chapter Two, it is reasonable to ask; if the atmospheric transmittance and path radiance are available to us will it be possible to do an atmospheric correction on the data such that the classification results can be improved? In order to answer this question, lets first look at what an atmospheric correction would consist of. To correct for the atmosphere an inverse type of operation is needed. This will involve changing the data from the digitized domain into the radiance domain, subtracting from it the estimated path radiance and then multiplying by the estimated inverse atmospheric transmittance matrix. By looking at (3.1) we can easily see that the resulting expression will be

$$\mathbf{Y} = \tau_a^{-1}(\mathbf{Z}-\mathbf{L}_p) = \mathbf{L}_s+\tau_a^{-1}\mathbf{N}(\mathbf{L}). \qquad (3.26)$$

where **N** represents all the noises introduced by the sensor system. For data taken under good atmospheric conditions the second term could be negligible compared to the signal term, $\mathbf{L}_s$. Now, if the classifier used is a Bayes minimum error pixel classifier the answer to the question is no. This is because as was shown in Chapter Two, this type of operations does not affect the percent of overlapping between the possible classes.

If it is desirable to estimate the reflectance of the ground based on the available data, the digitized data will have to be converted to the radiance domain. Once in the radiance domain all atmospheric effects present in the data have to be removed as mention earlier and then multiplied by the inverse solar irradiance matrix measured at the earth surface. Much has been done with this kind of calibration procedure [S2], which sounds very reasonable if a photo-interpretation method is to be used. But again, if the main concern of the user is to do an accurate estimation of the classification based only on the frame of data available, and using a quantitative approach then it makes no difference in the classification results to correct for the atmosphere or go to the reflectance domain.

Maxwell [M1] has made use of spatial filters as an alternative method of reducing the spectral noise and in that way improving the classification accuracy. In particular he made use of a moving average window which showed a classification improvement from 18.8 percent of error to 3.6 when it was applied to a noisy data set. He made the observation that although there was a significant improvement in the classification accuracy the edges of the

final images were blurred by the filter. Since a linear spatial filter like the moving average window will tend to blur the edges in the image, defined at the boundaries of one class to another (introducing possible misclassification), we decided to seek another kind of filter which could preserve a good classification accuracy in the overall image frame. A non-linear filter known as the median filter seemed to have these attributes [H2].

The implementation of a median filter can be understood in a similar way as the moving average window, but in the median filter case the pixel falling in the center of the window is replaced by the median value obtained from all the pixel values falling inside the window. Some preliminary results were obtained using a recursive separable median filter with a window of width three. Table 3.1 summarizes the results obtained when a four band multispectral image was corrupted with additive gaussian noise with standard deviation equal to seven. This noisy image was filtered with a recursive separable median filter and then a classification was performed and compared to the classifications obtained for the original image and the noisy image. The classification improvement after filtering was greater than twenty percent overall. Figures 3.14 - 3.16 show the classification results. One of the disadvantages of this filter is that the output statistics are far from trivial to obtain and closed form expressions are very difficult to find. Future work is planned to be done with this kind of filter and to compare it to the moving average window and other proposed non-linear

Table 3.1 Classification results for a separable recursive median filter.

Class	Percent of Correct Classification		
	Original	Noisy	Filtered
Soybeans	96.9	42.0	73.2
Corn	97.0	62.3	86.2
Oats	95.3	51.9	74.9
Wheat	97.3	63.3	83.4
Red cl	92.6	51.3	76.0
Alfalfa	94.9	79.3	88.0
Rye 1	95.7	50.5	86.2

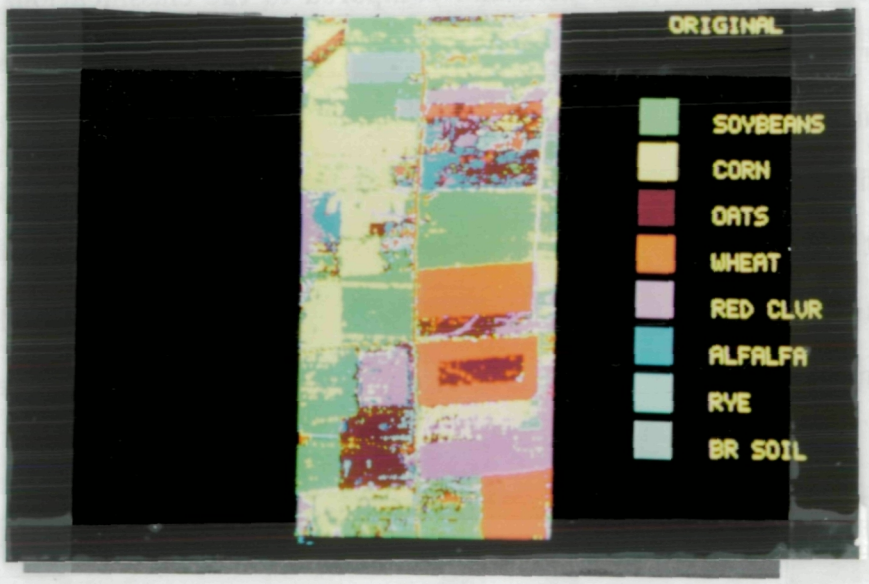

Figure 3.14 Classification results of the original data.

Figure 3.15 Classification results of the original data plus white additive gaussian noise, N(0,7).

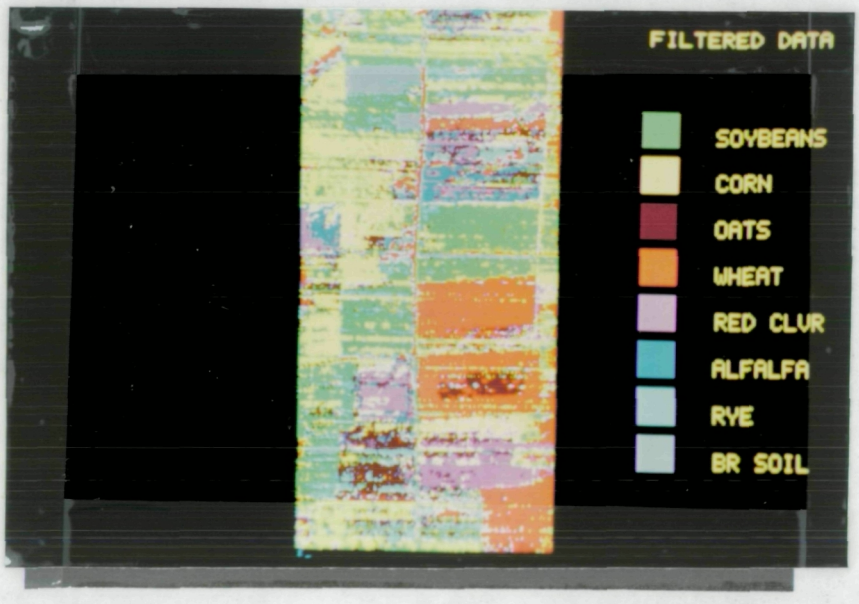

Figure 3.16 Classification results of noisy filtered data.

filters.

3.7 Observations

In this work a model for the data acquisition system in a multispectral scanner system like the one utilized by the LANDSAT satellites was presented. Since the shot noise introduced by the photodetectors in the sensor system is signal level dependent, an atmospheric model was adopted which could adequately describe the amount of radiation that gets into the sensors based on the atmospheric transmittance. An analysis was carried out to find the output spectral statistics in terms of the input signal statistics and the system parameters. This was integrated into a set of fortran programs that can be used to estimate the classification performance when supplied with the class statistics, noise levels introduced by the sensor system, the atmospheric transmittance, and the atmospheric path radiance.

Further topics to be considered in the improvement of this model are:

1- Relaxation of the assumption of relatively high input radiance arriving at the photodetector input, which allowed approximating the photodetector output by a gaussian distribution with parameters being signal level dependent.

2- Implementation of a non-constant atmospheric model.

3- Use of a path radiance model that considers the cover class under observation.

A library of programs called the Unified Scanner Analysis Package (USAP) had been developed at the Laboratory of Application of Remote Sensing

(LARS) to simulate a multispectral scanner in a more global way than the one presented in this thesis. This package has a weak point because it does not consider any atmospheric effects and it assumes the sensor noise to be the same in all spectral bands. The work done in this study could be easily appended to the USAP system developed at LARS in order to obtain a better simulation of the multispectral scanner system.

LIST OF REFERENCES

LIST OF REFERENCES

[B1] A. Bhattacharyya, "On a Measure of Divergence between Two Statistical Populations Defined by their Probability Distributions," Bulletin of the Calcuta Mathematical Society, V. 35, No. 3, September, 1943.

[D1] Davenport and Root, "An Introduction to the Theory of Random Signals and Noise," McGraw-Hill, New York, 1958.",

[D2] S.Q. Duntley, "The reduction of Apparent Contrast by the Atmosphere," J. Opt. Soc. Am. 38,179, 1948.

[E1] L. Elterman, "Vertical-Attenuation Model with Eight Surface Metereological Ranges 2 to 13 km," Report 70-0200, Air Force Cambridge Research Laboratory, 1970.

[F1] K. Fukunaga, "Introduction to Statistical Pattern Recognition," Academic Press, 1972.

[F2] K. Fukunaga and Krile, "Calculation of Recognition Error for Two Multivariate Gaussian Distributions," IEEE Transactions on Computers, March, 1969.

[F3] K. Fu, D. Landgrebe, and S. Phillips, "Information Processing of Remotely Sensed Data," Proceedings of the IEEE, April, 1969.

[G1] R.M. Gagliardi and S. Karp , "Optical Communications," John Wiley & Sons, 1976 .

[G2] M. Gupta, "Electrical Noise: Fundamentals & Sources," IEEE Press, 1977.

[H1] J. Harnage, and D. Landgrebe, "Landsat-D Thematic Mapper Technical Working Group," Final Report, NASA/Johnson Space Center, 1975.

[H2] T.S. Huang, "Two Dimensional Image Processing," Springer-Verlay Berlin Heidelberg, 1981.

[K1] R.K. Kiang, "Atmospheric Effects on Cluster Analysis," Proc. of Thirteenth International Symposioum on Remote Sensing of the Environment at the Environmental Research Institute of Michigan, 1979.

[M1] E.L. Maxwell, "Multivariate System Analysis of Multispectral Data," Photogram. Eng. Rem. Sens. 42, 1173, 1976.

[M2] B.G. Mobasseri, P.E. Anuta, C.D. McGillem, "A Parametric Model for Multispectral Scanners," IEEE Trans. on Geos. and Remote Sensing, Vol. GE-18, No. 2, April, 1980.

[O1] B.M. Oliver, "Thermal and Quantum Noise," Proc. IEEE, vol.53, pp. 436-454, May 1965.

[P1] A. Papoulis, "Probability, Random Variables and Stochastic Processes," McGraw-Hill, 1965.

[R1] S.O. Rice, "Mathematical Analysis of Random Noise," Bell System Tech J. Vols.23&24, 1964&1945.

[S1] V.V. Salomonson, "An Overview of Progress in the Design Implementation of Landsat D-System," IEEE Trans. Geosci. and Remote Sensing, vol.GE-18, April, 1980.

[S2] P.N. Slatter, "Remote Sensing Optics and Optical Systems," Addison-Wesley, 1980.

[S3] P.H. Swain and S.M. Davis, eds., "Remote Sensing: The Quantitative Approach," McGraw Hill, 1978.

[T1] R.E. Turner, "The Importance of Atmospheric Scattering in Remote Sensing," Proc. of Seventh Int. Symp. on Remote Sensing of the Environment at the Environmental Research Institute of Michigan, vol.3, 1971.

[V1] H.L. Vantrees, "Detection, Estimation, and Modulation Theory," John Wiley and Sons, 1968.

[W1]S.J. Whitsitt, "Error Estimation and Separability Measure in Feature Selection for Multiclass Pattern Recognition," LARS Technical Report 082377, 1977.

APPENDIX A
THEMATIC MAPPER

The Thematic Mapper (TM) is a scanning optical sensor aboard the Landsat 4 satellite, which is in a near polar sun-synchronous orbit at an altitude of 705 kilometers, with an earth swath scan of 185 Km wide. The TM is a second generation of earth resources space sensor. It works on the same basic principles of the Multispectral Scanners (MSS) aboard Landsat 1, 2, and 3. It is an image forming system where each pixel in the image is a vector consisting of a set of measurements from selected wavelengths regions in the spectrum. The TM was design so that it will achieve higher imagery resolution, sharper spectral separation, improved geometric fidelity and greater radiometric accuracy and resolution, compared to previous scanners. The spectral bands used by the TM are

band	range μm	description
1	.45-.52	blue
2	.52-.60	green
3	.63-.69	red
4	.76-.90	near infrared
5	1.55-1.75	middle infrared
6	2.08-2.35	middle infrared
7	10.4-122.5	thermal infrared

These bands were selected because they have proven to be helpful in the prediction of vegetation mapping, which is the principal mission of the Thematic Mapper. Silicon detectors are being used for the first 4 bands. The two middle infrared and thermal infrared bands use indium antimonide and mercury cadmiun-telluride detectors, respectively. The detectors of the latter three bands must be at low temperatures in order to preserve high SNR.

Harnage and Landgrebe [H1] have stated that classification accuracies are acceptable for most remote sensing applications when the fields of the scene are greater than 8 Instantaneous Fields of Views (IFOV) in size. With the TM IFOV of 30 meters, adequate crop estimation is more approachable in countries where the field sizes are smaller that the ones in USA.

A nominal equatorial crossing time of 9:30 AM has been chosen for Landsat 4 because it will provide less cloud cover and topographic information can be obtained from the shadows. It follows that a nominal equatorial solar zenith angle of 37.5 degrees will be achieved by the Thematic Mapper. For a detailed description of the Thematic Mapper design predicted performances see [H1,S1].

APPENDIX B

NON CONSTANT ATMOSPHERE

The non constant atmosphere considered here is one where the atmospheric transmittance and path radiance varies along the satellite path. This could be induced by inhomogeneity of aerosol and water vapor concentrations in the atmosphere. A model presented by Kiang [K1] that considers this fluctuations is given by

$$\mathbf{L} = \tau_a(\mathbf{t})\mathbf{L}_s + \mathbf{L}_p(\mathbf{t}) \tag{1}$$

where τ_a and $\mathbf{L}_p$ are the transmittance matrix and path radiance vector, respectively. Both of them are considered to be random and are functions of the optical thickness $\mathbf{t}$ which is also a random vector with mean value t_o. Let $\tau_o = \tau_a(t_o)$ and $L_{p_o} = L_p(t_o)$. Expanding $\mathbf{L}$ in a Taylor series of t about t_o.

$$\mathbf{L} = \tau_o\mathbf{L}_s + L_{p_o} + [(\frac{d\tau_a}{dt})_o\mathbf{L}_s + (\frac{dL_p}{dt})_o](\mathbf{t}-t_o) + \text{H.O.T.} \tag{3}$$

Assuming that the fluctuations of the optical thickness are small we can neglect the higher order terms and make the following approximation,

$$\mathbf{L} \simeq \tau_o\mathbf{L}_s + L_{p_o} + \gamma \tag{4}$$

which resembles the constant atmospheric model presented in Chapter 2 with the exception that there is an additive term γ which is due to the fluctuations of optical thickness. This term can be considered as a first order approximation to be the atmospheric noise. It has an expected value of

$$E[\gamma] = 0 \tag{5}$$

It then follows

$$E[\mathbf{L}] \simeq \tau_o E[\mathbf{L}_s] + \mathbf{L}_{p_o}$$

$$\Sigma_{\mathbf{L}} \simeq \tau_o \Sigma_{\mathbf{L}_s} \tau_o^t + \Sigma_\gamma$$

This model was not used in the present work because the statistics of the random variable γ were unknown.

APPENDIX C

SOFTWARE LISTING

```
      program mss
*****************************************************************
* This program simulates the statistical transformations that
* two input signals undergo at different stages of a
* multispectral scanner system  The signals for each class
* are characterized by the  covariance matrices and mean vectors
*   The program estimates the probability of misclassification and
* the Bhattacharyya distance between classes  The inputs to the
* program are
*   fname=output file name
*   tao=atmospheric optical thickness values
*   s=values that will adjust the actual noise levels.
*   mr=metereological range
*   factor=increment used by numerical integration
*   k=dimensionality to be used
*   ko=actual dimensionality of input statistics
*   index=ith coefficient in a to be modified
*   value1=starting value of a(index)
*   value2=final value of a(index)
*   step1=# of intervals used
*   cname(1&2)= input file with signal statistics
* Libraries used (IMSL) are used
*****************************************************************
      character*6 cname(2),fname
      real kx(25,2),mx(25,2),kys(21,2),eys(6,2),lp(6),t(5)
      real s(25,4),rmax(6),rmin(6),a(3),tao(5),k1(6),k2(6)

      data k1/2 309e-4,2 1533e-4,2.383e-4,1 7889e-4,1.7678e-4,11.7678e-4/
      data k2/ 74e-5,.53e-5, 45e-5,.35e-5, 72e-5,.92e-5/
      data lp/150 ,150 ,150.,150 ,150 ,150./
      data rmax/1.06e-3,2 54e-3,1 46e-3,3.26e-3,.64e-3,.467e-3/
      data rmin/0 ,0.,0 ,0 ,0 ,0 /
      data cname/'class1','class2'/
* read control file
      read(5,*) fname
      open(2,file=fname)
      rewind 2

1000  read(5,*,end=300) tao
      read(5,*) s,mr,factor,k,ko
      read(5,*) index,value1,value2,step1
      step=(value2-value1)/step1
      print'("factor=",f6 4)',factor
      write(6,*)
      kd=ko*(ko+1)/2
      kd1=k*(k+1)/2

* read input statistics for two classes
      do 1 i=1,2
      open(1,file=cname(i))
      rewind 1
      read(1,*) (kys(j,i),j=1,kd),(eys(j,i),j=1,ko)
      close(1)
1     continue

* set values of weighting coeff
      aindex=value1
      istep=nint(step1)
      if(value1 eq value2) istep=0
      do 2 iqv=0,istep
      a(index)=aindex+ iqv*step
      write(6,8) index,value1,value2,step1,a(index)
8     format(13,4f8 2)
      write(6,*)

* form cov matrices for shot,pream and quant noise
      theta=(37.5/360)*2 *3 14159
      do 3 i=1,k
      ia=1*(i-1)/2 + 1
      s(ia,1)=a(1)*k1(i)*sqrt(255./(rmax(i)-rmin(i)))
      s(ia,2)=a(2)*sqrt( (255 /rmax(i))*k2(i) )
      s(ia,3)=(a(3)**2)/12
      t(i)=exp(-1 *tao(i)/cos(theta))
3     continue
      if(iqv eq.0) then
      print'("metereological range    :",12)',mr
      write(6,*)
      print'("atmospheric transmittance ",10f6.3)',(t(i),i=1,k)
      write(6,*)
      endif

      do 500 ic=1,2
*
* form covariance matrix for signal
*
      do 100 ix=1,k
        pathr= lp(ix) *(1-t(ix))
        mx(ix,ic)=t(ix)*eys(ix,ic) + pathr

       do 75 iy=1,ix
         kk=ix*(ix-1)/2 + iy
         if(ix eq.iy) then
         x=t(ix)*kys(kk,ic)*t(iy)
         x=x+s(kk,1)**2*mx(ix,ic)+s(kk,2)**2.+s(kk,3)
         kx(kk,ic)=x
         else
         kx(kk,ic)=t(ix)*kys(kk,ic)*t(iy)
         endif
75     continue
100    continue
500    continue
c     call uswsm("sig1",4,kx(1,1),k,1)
c     call uswsm("sig2",4,kx(1,2),k,1)
      call diag(kx(1,1),kx(1,2),mx(1,1),mx(1,2),k,kd1,factor,a(index))
2     continue

      go to 1000
300   print'("end of file")'
      stop
      end
```

```
      subroutine diag(sig1,sig2,mv1,mv2,nd,nd1,factor,vindex)
c*****************************************************************
c* This subroutine does a simultaneous diagonalization on the two
c* input covariance matrices  The transformation used is also
c* applied to the mean vectors  It computes the Bayes error,
c* computes the Bhattacharyya
c* distance and the upper bound of the Bayes error stablished by
c* it.
c* SUBROUTINES CALLED.
c* subroutine errorand subroutines defined in the IMSL library
c*****************************************************************
      real mv1(nd),mv2(nd),sig1(nd1),sig2(nd1)
      real t(10,10),tt(10,10),wk1(200)
      real phi(10,10),wk(200),wkm(10,10),eval(50),dist(50)
      real evec(10,10),wka(10,10),res(10)
      jobn=2
      ix=10
      do 12 ix=1,nd
      do 12 iy=1,nd
   12 wkm(ix,iy)=0 0

c* find eigenvectors and eigenvalues of sigma1 -> eigenv,phi
      call eigrs(sig1,nd,jobn,eval,evec,ix,wk,ier)
      if(wk(1) gt 100 ) then
        print'(' performance index1=",f14.5)',wk(1)
        stop
      endif

c* form eval**(-.5)
      do 30 ix=1,nd
   30 wkm(ix,ix)=eval(ix)**(-.5)
c     call uswfm("evec1",5,evec,10,nd,nd,2)
c     call uswfm("eval**-.5",11,wkm,10,nd,nd,2)

c* form T= eval**(-.5) * evec-t
      do 40 ix=1,nd
        do 35 iy=1,nd
        sum=0 0
        do 33 i=1,nd
        sum=sum+wkm(ix,i)*evec(iy,i)
   33   continue
        t(ix,iy)=sum
        tt(iy,ix)=sum
   35   continue
   40 continue
c     call uswfm("T",1,t,10,nd,nd,2)

c* form t*sig2*tt   ->  tt
      call vmulsf(sig2,nd,tt,nd,10,wkm,10)
      call vmulff(t,wkm,nd,nd,nd,10,10,tt,10,ier)
c     call uswfm("k=T*sig2*TT",11,tt,10,nd,nd,2)

      call vcvtfs(tt,nd,10,wk)
c     call uswsm("K",1,wk,nd,2)

c* find eigenvectors and eigevalues of wk
      call eigrs(wk,nd,jobn,eval,evec,ix,wk1,ier)
      if(wk(1).gt 100 ) then
        print'("performance index2=",f14 5)',wk1(1)
        stop
      endif
c     call uswfm("evec of k",9,evec,10,nd,nd,2)
c     print'(' eigenvalues of K",10f14 5)',(eval(i),i=1,nd)

c* form phi=evec-t * t
      call vmulfm(evec,t,nd,nd,nd,10,10,phi,10,ier)
c     call uswfm("matrix trans ",13,phi,10,nd,nd,2)

c* form dist vector
      dc 60 i=1,nd
        mv2(i)=mv2(i)-mv1(i)
        sum=0.0
        do 50 j=1,nd
        tt(i,j)=phi(j,i)
        t(i,j)=phi(i,j)
   50   continue
   60 continue
      call vmulff(t,mv2,nd,nd,1,10,50,dist,50,ier)

c     call uswsm("sig1",4,sig1,nd,1)
c     call uswsm("sig2",4,sig2,nd,1)

c* form identity
c     call vmulsf(sig1,nd,tt,nd,10,wkm,10)
c     call vmulff(t,wkm,nd,nd,nd,10,10,wka,10,ier)
c     call uswfm("identity*",9,wka,10,nd,nd,1)

c* form eigenvalue matrix
c     call vmulsf(sig2,nd,tt,nd,10,wkm,10)
c     call vmulff(t,wkm,nd,nd,nd,10,10,wka,10,ier)
c     call uswfm("eigenvalues*",12,wka,10,nd,nd,1)


c* compute Bhattacharrya distance
      sdist=0
      do 100 i=1,nd
      dd=dist(i)**2/(2*(1 +eval(i)))
      dd=dd+ log((1.+eval(i))/2 ) -.5*log(eval(i))
      sdist=sdist+dd
  100 continue
      sdist=.5*sdist
      e1=exp(-1 *sdist)
      res(1)=sdist
      res(2)=e1*100
      res(3)=e1*50
      res(4)=erfc( sqrt(2*sdist)/sqrt(2.) )*50.
c     print'("u = ",f8.3)',sdist
c     e1=exp(-1.*sdist)
c     print'"  1 < .f. ",10x,"e <",f8 3)',e1*100.,100 *e1/2.

c* compute "actual" error
      call errest(sig1,sig2,tt,dist,eval,factor,nd,e1,e2,e,nf)
      res(5)=e1
      res(6)=e2
      res(7)=e
      res(8)=vindex
      res(9)=float(nf)
      write(6,1000) (res(i),i=1,9)
 1000 format("results ",5f12.5)
      write(6,*)

      write(2,*) (res(i),i=1,9)
      return
      end
```

```
      subroutine error(a,b,h,d,eig,factor,ndim,e1,e2,e,ic)
*     This subroutine is called by "diag".  It estimates the
*     probability of error between two classes by performing
*     a numerical integration over a single variable in the
*     frequency domain.  See Fukunaga and Krile.
      real a(ndim,2),b(ndim,2),h(ndim,2),d(ndim),eig(ndim)
c     print'("enter factor ndim eig d ")'
c     read(5,*) factor,ndim,eig,d
      write(6,*)
      print'("eigenvalues     ",10f9.3)',(eig(i),i=1,ndim)
      write(6,*)
      print'("distance vector ",10f9.3)',(d(i),i=1,ndim)
      write(6,*)
   11 format(10f9.3)
      ic=0
      e1=0
      e2=0
      pi=3.1415926554
      v1=1
      v2=.25
      v3=.5
      do 5 i=1,ndim
        dist=d(i)
        a(i,1)=1 -1./eig(i)
        a(i,2)=eig(i)-1
        b(i,1)=(1 /eig(i))*dist
        b(i,2)=sqrt(eig(i))*dist
        b12=b(i,1)**2
        b22=b(i,2)**2
        lambda=log(eig(i))
        h(i,1)=b12/(1 -a(i,1)) + lambda
        h(i,2)=-1 *b22/(1 +a(i,2)) + lambda
    5 continue

    1 continue
      ic=ic+1
      w=ic*factor
      w2=w**2
      pmag1=1.
      pang1=0.
      pmag2=1
      pang2=0

      do 10 i=1,ndim
        a12=a(i,1)**2
        a22=a(i,2)**2
        b12=b(i,1)**2
        b22=b(i,2)**2
        aw1=a(i,1)*w
        aw2=a(i,2)*w
        a1w2=a(i,1)*w2
        a2w2=a(i,2)*w2
        dm1=v1+w2*a12
        dm2=v1+w2*a22
        dum1= atan(aw1)-w*((h(i,1)+b12*a1w2/dm1))
        dum2= atan(aw2)-w*((h(i,2)+b22*a2w2/dm2))
        pang1=pang1 + dum1
        pang2=pang2 + dum2
        pmag1=pmag1*(dm1**(-v2)*exp(-v3*b12*w2/dm1))
        pmag2=pmag2*(dm2**(-v2)*exp(-v3*b22*w2/dm2))
   10 continue
      pang1=.5*pang1
      pang2=.5*pang2
      phi1=(pmag1/w)*sin(pang1)
      phi2=(pmag2/w)*sin(pang2)
c     print'("ang,mag,phi2,w",4f14.5)',pang2,pmag2,phi2,w
      e1=e1+phi1
      e2=e2+phi2
      pmag=pmag1+pmag2
      if(pmag gt..0001) go to 1

      e1= .5 - (1./pi)*e1*factor
      e1= (1  - e1)*100
      e2= ( 5 - (1 /pi)*e2*factor)*100
      e= (e1+e2)/2
c     print'("e1,e2,e,n",3f7.2,i5)',e1,e2,e,ic
      return
      end
```